Received: 16 May 2023 | Revised: 3 October 2023 | Accepted: 7 November 2023

DOI: 10.1002/nbm.5082

RESEARCH ARTICLE

NMR IN BIOMEDICINE WILEY

Four-dimensional flow MRI for quantitative assessment of cerebrospinal fluid dynamics: Status and opportunities

Leonardo A. Rivera-Rivera[1,2] | Tomas Vikner[2,3] | Laura Eisenmenger[4] | Sterling C. Johnson[1] | Kevin M. Johnson[2,4]

[1]Department of Medicine, University of Wisconsin School of Medicine and Public Health, Madison, Wisconsin, USA

[2]Department of Medical Physics, University of Wisconsin School of Medicine and Public Health, Madison, Wisconsin, USA

[3]Department of Radiation Sciences, Radiation Physics and Biomedical Engineering, Umeå University, Umeå, Sweden

[4]Department of Radiology, University of Wisconsin School of Medicine and Public Health, Madison, Wisconsin, USA

Correspondence
Leonardo A. Rivera-Rivera, University of Wisconsin-Madison, 600 Highland Ave CSC, K6/418 (MC4760), Madison, WI 53792, USA.
Email: larivera@wisc.edu

Funding information
Alzheimer's Association, Grant/Award Number: AARFD-20-678095; National Center for Advancing Translational Sciences; National Institute of Neurological Disorders and Stroke; National Institute on Aging; National Institutes of Health, Grant/Award Numbers: UL1TR002373, KL2TR002374, R21NS125094, R21AG077337, P30AG062715, R01AG021155, R01AG027161, R01AG075788

Neurological disorders can manifest with altered neurofluid dynamics in different compartments of the central nervous system. These include alterations in cerebral blood flow, cerebrospinal fluid (CSF) flow, and tissue biomechanics. Noninvasive quantitative assessment of neurofluid flow and tissue motion is feasible with phase contrast magnetic resonance imaging (PC MRI). While two-dimensional (2D) PC MRI is routinely utilized in research and clinical settings to assess flow dynamics through a single imaging slice, comprehensive neurofluid dynamic assessment can be limited or impractical. Recently, four-dimensional (4D) flow MRI (or time-resolved three-dimensional PC with three-directional velocity encoding) has emerged as a powerful extension of 2D PC, allowing for large volumetric coverage of fluid velocities at high spatiotemporal resolution within clinically reasonable scan times. Yet, most 4D flow studies have focused on blood flow imaging. Characterizing CSF flow dynamics with 4D flow (i.e., 4D CSF flow) is of high interest to understand normal brain and spine physiology, but also to study neurological disorders such as dysfunctional brain metabolite waste clearance, where CSF dynamics appear to play an important role. However, 4D CSF flow imaging is challenged by the long T1 time of CSF and slower velocities compared with blood flow, which can result in longer scan times from low flip angles and extended motion-sensitive gradients, hindering clinical adoption. In this work, we review the state of 4D CSF flow MRI including challenges, novel solutions from current research and ongoing needs, examples of clinical and research applications, and discuss an outlook on the future of 4D CSF flow.

KEYWORDS
4D flow, CSF, dynamics, motion, MRI, phase contrast, V_{enc}

Abbreviations used: AD, Alzheimer's disease; AGs, arachnoid granulations; BBB, blood–brain barrier; bSSFP, balanced steady-state free precession; CA, cerebral aqueduct; CBF, cerebral blood flow; CFD, computational fluid dynamics; CMI, Chiari malformation type I; CNN, convolutional neural network; CNS, central nervous system; CP, choroid plexus; CSF, cerebrospinal fluid; ECG, electrocardiography; EPI, echo planar imaging; FM, foramen magnum; FMa, foramen of Magendie; FMo, foramen of Monro; ICC, intraclass correlation coefficient; ICP, intracranial pressure; IIH, idiopathic intracranial hypertension; INPH, idiopathic normal pressure hydrocephalus; IPAD, intramural periarterial drainage pathway; ISF, interstitial fluid; MRI, magnetic resonance imaging; MV, mean velocity; OSI, oscillatory shear index; OSS, oscillatory shear stress; PC, phase contrast; PDV, peak diastolic velocity; PET, positron emission tomography; PGSE, pulse-gradient-spin-echo; PPG, peripheral pulse gating; PSV, peak systolic velocity; PVS, perivascular spaces; ROI, region of interest; SAS, subarachnoid space; SIH, spontaneous intracranial hypotension; SNR, signal-to-noise ratio; SPGR, spoiled gradient echo; SV, stroke volume; TE, echo time; TR, repetition time; V_{enc}, velocity encoding; WSS, wall shear stress.

Leonardo A. Rivera-Rivera and Tomas Vikner contributed equally to this work.

1 | INTRODUCTION

Cerebrospinal fluid (CSF) dynamics are increasingly studied to understand healthy brain and spine physiology, and the pathophysiology of cerebrovascular and neurodegenerative diseases, including stroke,[1] intracranial hypotension and hypertension,[2] elevated intracranial pressure (ICP),[3] idiopathic normal pressure hydrocephalus (INPH),[4–6] Alzheimer's disease (AD),[7–9] and Chiari malformations.[10–12] The human central nervous system (CNS) contains approximately 130 to 150 mL of CSF[13] located in the ventricles, in perivascular spaces (PVS), and in the subarachnoid space (SAS), including the spinal canal, which is a major contributor to CSF compliance.[2] Because of the constant space of the cranium, CSF oscillations are tightly coupled with arterial and venous pressure and flow dynamics,[14,15] partially driven by cardiac and respiratory pulsations. While the importance of CSF for supporting the brain with mechanical protection and buoyancy is well established, recent developments have highlighted the role of CSF in managing CNS homeostasis and metabolic waste clearance.[9,16] However, several knowledge gaps remain regarding normal CSF physiology and the role of altered CSF dynamics in neurodegenerative diseases, largely because of a lack of noninvasive imaging methods to study CSF flow in humans.

In the healthy brain, approximately 25 mL of CSF is contained within the ventricles, while the remaining part resides in SAS and PVS compartments.[13] The "third circulation" describes how CSF is produced in the ventricles by the choroid plexus (CP), flows through the cerebral aqueduct (CA) to the fourth ventricle, down through the foramens of Magendie (FMa) and Luschka, for distribution into the SAS and spinal canal.[13,17,18] However, discoveries of retrograde flow in the CA (i.e., towards the lateral ventricles) question such models.[19,20] While still being debated, most of the evidence suggests a majority of CSF (~80%) is produced by the CP, and the remaining fraction is produced by interstitial fluid (ISF) or by influx across the blood–brain barrier (BBB),[13,17] potentially depending on biological factors (e.g., age, sex) and brain state (e.g., wake/sleep).[13] Finally, CSF is thought to be reabsorbed into venous blood, by lymphatic vessels, arachnoid granulations (AGs), or both.[21,22] Methods to simultaneously assess flow in multiple CSF compartments could clarify discrepancies among CSF circulation models. Importantly, CSF velocities have a wide range (Table 1) and are not necessarily unidirectional, but pulsatile. For example, while large peak velocities are observed in the CA over the cardiac cycle (±30 cm/s), extremely slow flows can be expected in the SAS CSF (e.g., <1 cm/s).

Evidence from animal studies indicating the presence of brain metabolite waste-clearance systems has also changed our understanding of CSF circulation, with potential implications for AD and other proteinopathies. The glymphatic pathway[9,40] and the intramural periarterial drainage pathway (IPAD)[41,42] both describe how CSF enters the brain along PVS, for mixing with ISF in the parenchyma, and exits along venous PVS (glymphatics) or along basement membranes of penetrating arteries (IPAD). Other models suggest that mixing of CSF and ISF happens directly in the PVS compartment.[43,44] Clearance systems are thought to compensate for the fact that the brain lacks a lymphatic system and is separated from the bloodstream by the BBB. While still debated, cerebral blood flow (CBF) dynamics, including low-frequency vasomotion (~0.05–0.1 Hz) evoked by neuronal activity,[1,45,46] respiratory-induced CBF-CSF motion coupling[47–49] (~0.25–0.4 Hz), and cardiac-related vessel wall pulsations[50–52] (~0.8–1.2 Hz), could function as pumping mechanisms that propel CSF through the SAS and along PVS, for CSF-ISF exchange in the parenchyma or directly in the PVS.

Despite increasing evidence of impaired CSF-mediated waste clearance in neurological disorders, human studies on this matter are scarce, largely because of a lack of noninvasive methods to quantify flow in CSF compartments of interest. To obtain quantitative flow estimates in the human brain, velocity-sensitive phase contrast magnetic resonance imaging (PC MRI) sequences are typically employed. In PC MRI, velocity encoding is based on the observation that changes in the MRI signal along a magnetic field gradient are directly related to the flow velocity.[53–57] In two-dimensional (2D) PC, an imaging slice is manually placed by the operator prior to the MRI acquisition. Using bipolar velocity-encoding gradients, velocity-dependent phase changes can be detected by playing out two acquisitions with different velocity-encoding gradients but otherwise identical imaging parameters. Subtraction of the phase images allows for removal of the unknown background phase and calculation of velocity images.[55] Quantitative measures of fluid velocities (e.g., cm/s) and flow rates (e.g., mL/s) can be derived from ungated 2D PC MRI using semiautomatic tools. To derive markers of flow dynamics such as peak systolic velocity (PSV) and stroke volume (SV), cardiac-resolved (e.g., electrocardiography [ECG]-gated) 2D PC MRI can be utilized.

2D PC studies have linked CSF dynamics to regional brain volumes,[58] hydrocephalus and INPH,[4,5] idiopathic intracranial hypertension (IIH),[59] spontaneous intracranial hypotension (SIH),[60] Chiari malformation type I (CMI),[61,62] and AD.[7] Typically, 2D PC studies have assessed flow in the CA, the foramens, and the spinal canal (Figure 1), regions where a single imaging slice could be sufficient and where 2D PC is a simple way to achieve quick and reliable results. However, comprehensive assessment of CSF dynamics with 2D PC may be impractical for regions of interest (ROIs) with large volumetric coverage and varying flow direction (e.g., the SAS), or for acquiring flow along multiple segments of relatively straight channels, like the CA[39] and spinal canal.[37] While prescribing multiple 2D PC scans orthogonal to the flow direction is an option, this would be time consuming and could introduce confounding variability if the slices are acquired at different heartbeat ensembles and respiration cycles. These challenges especially hinder the potential to study CSF dynamics in relation to brain clearance, where large (e.g., SAS) or widely spread out (e.g., dilated PVS) compartments are of interest.

Four-dimensional flow MRI (4D flow MRI), or time-resolved three-dimensional (3D) PC with three-directional velocity encoding, is an attractive alternative for comprehensive assessment of CSF dynamics over large imaging volumes. In addition to large coverage, the 3D velocity encoding allows for derivation of various parameters linked to CSF dynamics, such as streamlines, rotation fields, and shear stress. However, while

TABLE 1 Summary of four-dimensional (4D) flow MRI studies with a focus on cerebrospinal fluid (CSF) dynamics.

Reference	Subjects	CSF ROIs	4D flow markers	Res/frames/time	Field/v_{enc}	Summary/conclusions
Santini et al. 2009[23]	Spherical phantom; 2 HV	Spinal canal C3–C5	Streamlines	1.1 × 1.1 × 2 mm NS 20 min	1.5 T; 10 cm/s	bSSFP 4D flow MRI yields higher SNR in CSF than SPGR sequences
Bunck et al. 2011[24]	10 HV; 4 CMI/CCS	FM, spinal canal C1–C7	Streamlines, PSV, PDV	1.5 mm isotropic 8–14 frames 8–14 min	1.5 T; 10–20 cm/s	4D flow may distinguish physiological/pathophysiological CSF dynamics
Odeen et al. 2011[25]	Flow phantom; 5 HV	LV, 3V, 4V, CA, FMa	Velocity magnitude and significant flow connectivity[a]	2.1 × 1.6 × 1.6 mm 10–13 frames 14 min	3 T; 4–5 cm/s	Semiautomatic 4D flow connectivity analysis may identify CSF occlusions
Bunck et al. 2012[12]	10 HV; 20 CMI	FM, spinal canal C1–C7	Streamlines, PSV, PDV, PSF, PDF	1.5 mm isotropic 12–14 frames 8–14 min	1.5 T; 20 cm/s	4D flow could aid identify CMI patients who would benefit from surgery
Stadlbauer et al. 2012[26]	21 HV; 21 hydrocephalus	LV, 3V, 4V, CA, FMo	Velocity fields, MV, PSV	NS 12 frames 4.3–6.7 min	1.5 T; 2–5 cm/s	Altered CSF dynamics are observed in various kinds of hydrocephalus
Yiallourou et al. 2012[27]	4 CMI; 3 HV	FM, spinal canal C1–C7	Velocity fields, PSV, PDV, SV	1.5 mm isotropic 7–10 frames 8–14 min	1.5 T; 10–20 cm/s	4D flow and CFD could inform on CSF dynamics in health and disease
Matsumae et al. 2014[28]	11 HV; 1 CMI; 1 hydrocephalus	LV, 3V, 4V, CA, IPC, PPC, CM, SF, CSAS	Velocity fields, pressure gradients	1.96 mm isotropic 32 frames NS	1.5 T; 5 cm/s	Velocity and pressure fields may improve our view of normal CSF flow and help classify patients
Hirayama et al. 2015[29]	Flow phantom; 6 HV; 2 AC	LM, AC proximity	Velocity fields, pressure gradients	1.96 mm isotropic 32 frames NS	1.5 T; 5 cm/s	4D flow and time-SLIP provide complementary information on CSF dynamics
Pahlavian et al. 2015[30]	Subj.-specific phantom; 1 CMI; 1 HV	FM, spinal canal C1–C7	PSV magnitude fields, PSV at ROIs	1.5 mm isotropic 10–13 frames 8–14 min	1.5 T; 10–20 cm/s	4D flow show much larger PSV magnitudes than CFD
Pahlavian et al. 2016[31]	Subj.-specific phantom	FM, spinal canal C1–C7	Velocity/PSV/PDV fields, PSV at ROIs	1.0 × 1.0 × 1.5 mm 16 frames NS	1.5 T; 15 cm/s	4D flow/CFD do agree at time frames near systolic diastolic and peak flows
Thyagaraj et al. 2018[32]	Subj.-specific phantom	FM, spinal canal C1–C7	PSV fields and PSV and EDV vs. distance from the FM	1.0 mm isotropic 16 frames 15 min	3 T; 15 cm/s	In vitro models can be used to test CSF protocols for CMI across different MRI scanners
Takizawa et al. 2017[33]	19 HV; 1 INPH; 7 AD	CA	Velocity fields, pressure gradients, rotation	1.96 mm isotropic 32 frames 32 min	1.5 T; 5–30 cm/s	Hyperdynamic 4D flow CSF motion in both INPH and AD
Takizawa et al. 2018[34]	11 HV	LV, 3V, 4V, CSAS	Velocity fields, pressure gradients, MV, acceleration	1.96 mm isotropic 32 frames NS	1.5 T; 5 cm/s	Velocity/acceleration at ROIs questions the CP as origin of CSF pulsations
Brandner et al. 2018[35]	12 AS; 10 HV	LV, 3V, 4V, CA, FMo	Preoperative and postoperative velocity fields, MV, PSV	1.5 mm isotropic 12 + frames 10 min	3 T; 3 cm/s	4D flow has potential to evaluate flow changes after CA stenosis surgery
Yatsushiro et al. 2018[36]	13 INPH; 13 young HV; 13 elderly HV	LV, 3V, 4V, PPC, FM, LF	Waveform cross-correlation and time-delay maps	1.94 × 1.94 × 0.98 32 frames 30 min	1.5 T; 5–70 cm/s	Young, elderly, and INPH show different delay time and correlation maps

(Continues)

TABLE 1 (Continued)

Reference	Subjects	CSF ROIs	4D flow markers	Res/frames/time	Field/v_{enc}	Summary/conclusions
Jaeger et al. 2020[37]	20 HV	Spinal canal C1-L1	Streamlines, PSV, net flow, forward flow, backward flow	1.2–1.5 isotropic 15 frames NS	3 T; 15 cm/s	CSE acceleration 6 for spinal canal in CMI/SM reduces scan time by 40%
Yamada et al. 2020[5]	9 HV; 41 INPH; 23 AD/INPH	IPC, PMC, PPC, CA, FM FMa, FMo, C2	Streamlines, SV, WSS, reversed flow	1.0 × 1.0 × 1.3 mm 20 frames 10 min	3 T; 5 cm/s	CA shear stress increases progressively from HV, to AD/INPH, to pure INPH
Yamada et al. 2021[38]	9 HV; 41 INPH; 23 AD/INPH	CA, IPC, FM FMa, FMo	Streamlines, WSS, OSS, OSI	1.0 × 1.0 × 1.3 mm 20 frames 10 min	3 T; 5 cm/s	OSS could be better than OSI and WSS in INPH, etc.
Yavuz ilik et al. 2021[39]	10 NPH	CA	Corrected vs. uncorrected velocity fields, net flow	1.0 × 1.0 × 1.0 mm 8 frames 10 min	3 T; 5 cm/s	WPC most efficient for reducing phase offset errors
Williams et al. 2021[10]	Subject-specific phantom	FM, spinal canal C1–C7	PSV from 4D and 2D PC (3 scans/center; 5 centers)	1.5 mm isotropic 16 frames 15 min	3 T; 15 cm/s	High PSVs in CMI model. Inter-scanner variability a central source of error

Note: Cardiac-gated velocities were acquired in all studies, but not specified (NS) in some. Subject-specific phantoms indicate that the phantom geometry is based on subject-specific anatomy (e.g., anatomical scans). In case of both subjects and phantoms, the v_{enc} is specified for the subjects.
Abbreviations: **Subjects:** AC, arachnoid cyst; AD, Alzheimer's disease; CA, aqueduct stenosis; CCS, cervical canal stenosis; CMI, Chiari I malformation; HV, healthy volunteers; INPH, idiopathic normal pressure hydrocephalus. **Regions of interest (ROIs):** CA, cerebral aqueduct; CM, cisterna magna; CSAS, convexity SAS; FM, foramen magnum; FMa, foramen of Magendie; FMo, foramen of Monro; IPC, interpeduncular cistern; LF, longitudinal fissure; LM, Liliequist membrane; LV, lateral ventricle; PMC, premedullary cistern; PPC, prepontine cistern; SF, sylvian fissure; V, ventricle. **Four-dimensional (4D) flow markers:** MV (cardiac cycle average), mean velocity; OSI, oscillatory shear index; OSS, oscillatory shear stress; PDF, peak diastolic flow; PDV, peak diastolic velocity; PSF, peak systolic flow; PSV, peak systolic velocity; ROI, region of interest; SV, stroke volume; WSS, wall shear stress. **Res/phases/time:** Spatial resolution (acquired if both specified), phases/cardiac cycle, acquisition time. **Summary/conclusions:** bSSFP, balanced steady-state free precession; CFD, computational fluid dynamics; CP, choroid plexus; SM, syringomyelia; SNR, signal-to-noise ratio; SPGR, spoiled gradient echo; time-SLIP, time-spatial labeling inversion pulse; WPC, whole polynomial correction.
[a]A flow threshold was used to obtain binary three-dimensional CSF connectivity volumes (excluding low-flow voxels).

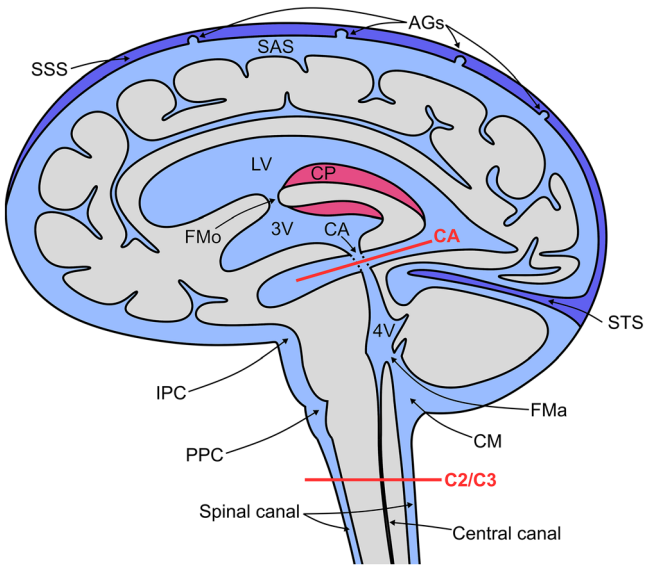

FIGURE 1 Overview of the cerebrospinal fluid (CSF) circulation system. The red planes indicate regions that are commonly investigated using two-dimensional (2D) phase contrast (PC) MRI, that is, the cerebral aqueduct (CA) and the spinal canal at the C2/C3 level. Four-dimensional (4D) flow MRI allows for simultaneous assessment of CSF dynamics in large regions with varying flow directions, such as the subarachnoid space (SAS), in addition to compartments commonly investigated by 2D PC. 3V, third ventricle; 4V, fourth ventricle; AGs, arachnoid granulations; CM, cisterna magna; CP,choroid plexus; FMa, foramen of Magendie; FMo, foramen of Monro; IPC, intrapeduncular cistern; LV, lateral ventricle; PPC, prepontine cistern; SSS, superior sagittal sinus; STS, straight sinus.

4D flow MRI has been extensively used in various vascular territories including thoracic,[63] abdominal,[64] neck,[65] and head[66–69] applications, studies on CSF dynamics are still scarce, largely because of challenges associated with imaging CSF instead of blood flow. In this work, we review the current state of 4D flow MRI of CSF (here referred to as 4D CSF flow). Specifically, we (1) identify challenges hindering 4D CSF flow imaging; (2) describe state-of-the-art solutions proposed by the research community to facilitate 4D CSF flow implementation; (3) provide an overview of clinical and research applications; and (4) conclude with ongoing needs and an outlook on the future of 4D CSF flow MRI.

2 | 4D CSF FLOW IMAGING

4D flow acquisitions are an extension of time-resolved 2D PC MRI on which 3D PC with three-directional velocity encoding is performed, typically for the three orthogonal x-, y-, and z-directions (Vx, Vy, and Vz).[63] A standard 4D flow MRI experiment requires four measurements, one for each velocity-encoded direction and a reference measurement to remove phase offsets.[54] The large amount of data required for 4D flow typically extends scan times and has historically hindered its clinical adoption. Recent advances in MRI system hardware and software have enabled 4D flow in clinically feasible scan times. These include faster, stronger, and higher fidelity imaging gradients for efficient non-Cartesian trajectories, phased array receiver technology with a greater number of elements for parallel imaging, and improved reconstruction methods such as compressed sensing and, more recently, deep learning. 4D flow allows for volumetric angiographic and quantitative assessment of flow velocities in a single acquisition, enabling visualization and quantification of complex flow fields.[63] The velocity field is captured throughout the length of the scan, enabling prospective or retrospective binning at multiple phases of the dynamics of interest (e.g., cardiac[55,70] or respiratory[71–73] cycles, or real-time[74,75]). Promising clinical studies and increased vendor interest have led to widespread availability of 4D flow in modern MRI systems, including postprocessing solutions. While clinical implementation of 4D flow has largely focused on large vascular territories[63,64] (e.g., aorta, pulmonary veins, portal veins), neurovascular applications are also increasing[66–69] (Figure 2). Neurovascular 4D flow requires high spatiotemporal resolution to detect blood flow in smaller structures.[76,77] Advances in neurovascular 4D flow acquisition,[76–79] reconstruction,[80,81] and the development of postprocessing[82–85] tools have turned 4D flow MRI into a versatile technique for the assessment of CBF dynamics. This includes derivation of a large number of hemodynamic biomarkers (reviewed elsewhere).[67,68,80,84,86–92] Importantly, 4D CSF flow imaging also demands high spatiotemporal resolution to quantify CSF dynamics across small and widespread structures (e.g., SAS, PVS). 4D CSF flow imaging is further challenged by the long T1 of CSF and the lower velocities associated with CSF motion, which leads to increased scan times. The clinical value of 4D CSF flow imaging has yet to be determined; however, it is an active area of research where methodologies are being developed to allow clinically feasible scan times and the derivation of useful biomarkers. Some evidence already supports 4D CSF flow as a tool that can provide accurate measures of CSF dynamics. Using anatomically detailed 3D printed models of the cervical SAS, researchers have observed good agreement between computational fluid dynamics (CFD) models and 4D CSF flow in terms of flow spatial distributions and peak through-plane velocities.[31] In a clinical research setting, 4D CSF flow has great potential as a tool with which to study brain-clearance phenomena in humans, including testing hypotheses linking CSF flow to models such as glymphatics,[9,40] IPAD,[41,42] and others[43,44] (Figure 3). In the following sections, we will discuss challenges, technological advances in the field, and clinical and research applications of 4D CSF imaging.

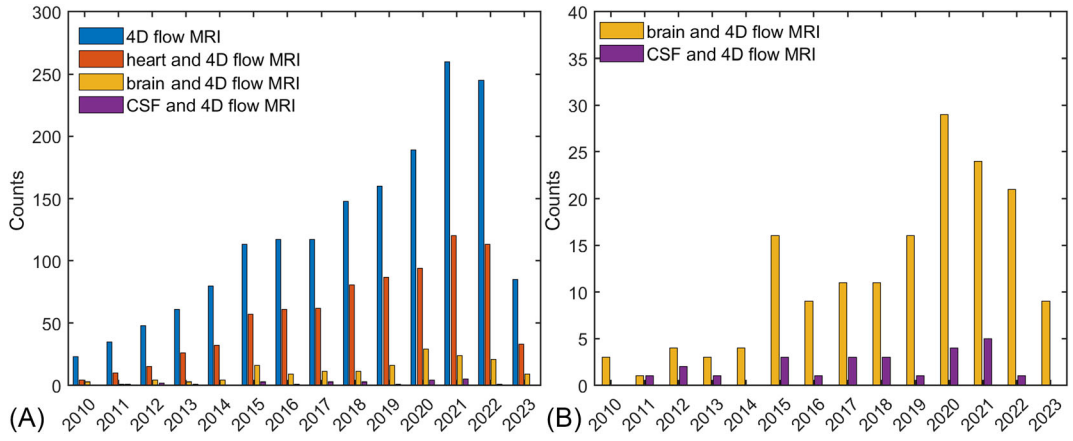

FIGURE 2 (A) Results of publication counts in PubMed after searching for "4D flow MRI", "heart AND 4D flow MRI", "brain AND 4D flow MRI", and "CSF AND 4D flow MRI". From 2010 to April 2023, the publication counts were: 1681, 795, 161, and 25, respectively, for each topic. (B) The same results for "brain AND 4D flow MRI" and "CSF AND 4D flow MRI". While the number of four-dimensional flow magnetic resonance imaging (4D flow MRI) publications continues to increase, a very small number of "CSF AND 4D flow MRI" publications was reported, displaying a small growth in counts per year.

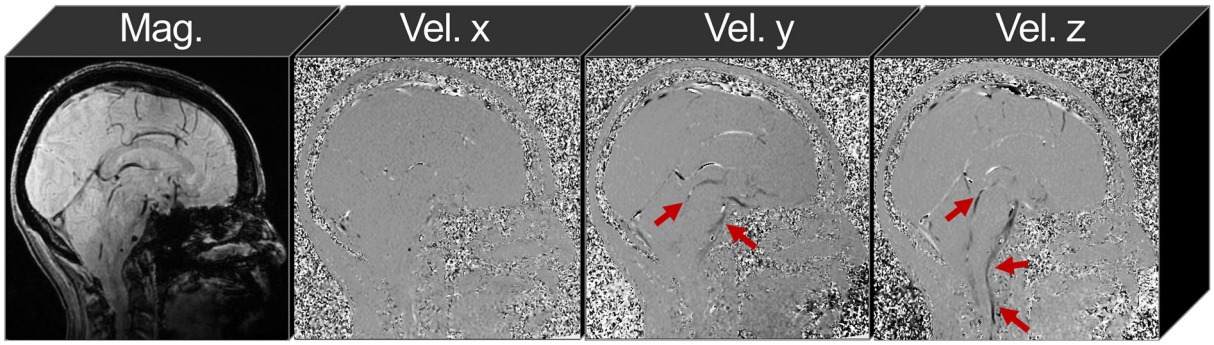

FIGURE 3 Example of magnitude (Mag.) and velocity (Vel.) images in the sagittal view from a four-dimensional cerebrospinal fluid (4D CSF) flow scan. Image parameters included: imaging volume = 25.6 × 25.6 × 4 cm^3, acquired resolution = 1 mm isotropic, TR/TE = 12/7 ms, flip angle = 3°, prospectively cardiac-gated (20-time frame interpolation), velocity encoding = 5 cm/s, scan time ~10 min. Structural and velocity data can allow for assessment of flow rates, relative pressure, pulse wave velocity, visualization of streamlines and particle trace, cardiac- and respiratory-motion flow contributions, and so forth. In this example, CSF motion can be observed (red arrows) across the cerebral aqueduct, foramen magnum, and subarachnoid space of the spinal cord. Data are from a 76-year-old study participant who is amyloid-beta positive from Pittsburgh compound B PET (PiB PET). 4D CSF flow has the potential to study CSF motion related to dysfunctional brain waste clearance in various proteinopathies, such as Alzheimer's disease.

2.1 | Challenges of 4D CSF flow imaging

Quantitative MRI is susceptible to imaging artifacts that can hinder its clinical value. Sources of error in 4D flow can originate from T2* decay, gradient nonlinearity, higher order motion (e.g., acceleration), concomitant gradients, flow ghosting, respiratory motion, velocity aliasing, eddy currents, intravoxel dephasing, chemical shift, reconstruction imaging errors, incomplete spoiling, partial volume effects, and so forth. Demands for higher spatiotemporal resolution can increase the probability for artifacts. Here, we focus on some challenges currently limiting fast and robust 4D CSF flow imaging. These include low signal-to-noise ratio (SNR) because of the long T1 of CSF and extended acquisition times from lower velocities, characteristic of CSF.

2.1.1 | T1 relaxation of CSF

At a field strength of 3.0 T, the estimated T1 relaxation value for blood[93] is ~1.6 s, while for CSF[94,95] T1 is much longer at ~4.5 s. The long T1 relaxation of CSF, indicative of the mostly free water in CSF, leads to slow regrowth of the longitudinal magnetization (M_z). The effects of CSF T1 on the 4D flow signal can be studied by considering the signal model of a spoiled gradient echo (SPGR) sequence.[96,97] SPGR sequences are frequently used in 4D flow experiments because of their short echo time (TE), short repetition time (TR), and well described relationships between velocity and phase. For a TR of 10 ms and Ernst flip angles for blood and CSF, the SPGR model dictates that $M_{z,CSF}$ ~60% $M_{z,blood}$ and $M_{xy,CSF}$ ~36% $M_{xy,blood}$. The SPGR 4D flow signal for CSF is significantly lower than for blood, resulting in CSF flow images with lower SNR. The velocity-to-noise ratio[98] (VNR), another important parameter, is proportional to SNR and inversely proportional to the encoding velocity. In CSF flow imaging, lowering the encoding velocity increases VNR, but such VNR gains are likely balanced by the lower CSF flow velocities. SNR still suffers primarily from the long T1 of CSF. To increase SNR of 4D CSF flow, higher field strengths or lower flip angles and longer acquisition times are typically necessary.

One way to increase SNR in CSF flow imaging is to use balanced steady-state free precession (bSSFP) imaging instead of SPGR.[23,99,100] bSSFP provides high signal for both blood and CSF. While SPGR contrast depends primarily on T1 and T2*, in bSSFP imaging, contrast is mixed and described by the ratio of T2/T1.[101] Considering the high T2/T1 ratio of CSF[102] at 3.0 T, bSSFP seems advantageous for 4D CSF flow imaging. 2D PC MRI experiments have demonstrated SNR increases of up to 63% for blood[100] and 350% for CSF[99] flow using bSSFP compared with SPGR. Further, such SNR increases may allow for a higher acceleration factor. Low CSF flow velocities reduce sensitivity to inflow enhancement in SPGR 4D flow acquisitions.[103] Compared with SPGR, inflow-dependent signal enhancement is less of an issue in bSSFP because of the high SNR, which is also beneficial for the segmentation of ROIs from magnitude data. bSSFP 4D flow has been successfully demonstrated in phantom experiments and utilized for the assessment of slow flows in veins and CSF (Figure 4).[23] While flow phantom data showed excellent agreement between bSSFP and SPGR ($R^2 = 0.998$), human experiments revealed that peak velocities were significantly underestimated because of the low temporal resolution of bSSFP compared with SPGR, despite the high SNR gains. The lower temporal resolution was partially due to requirements to balance the applied gradients. In bSSFP imaging it is not straightforward to obtain interleaved velocity encoding without lengthening the TR or

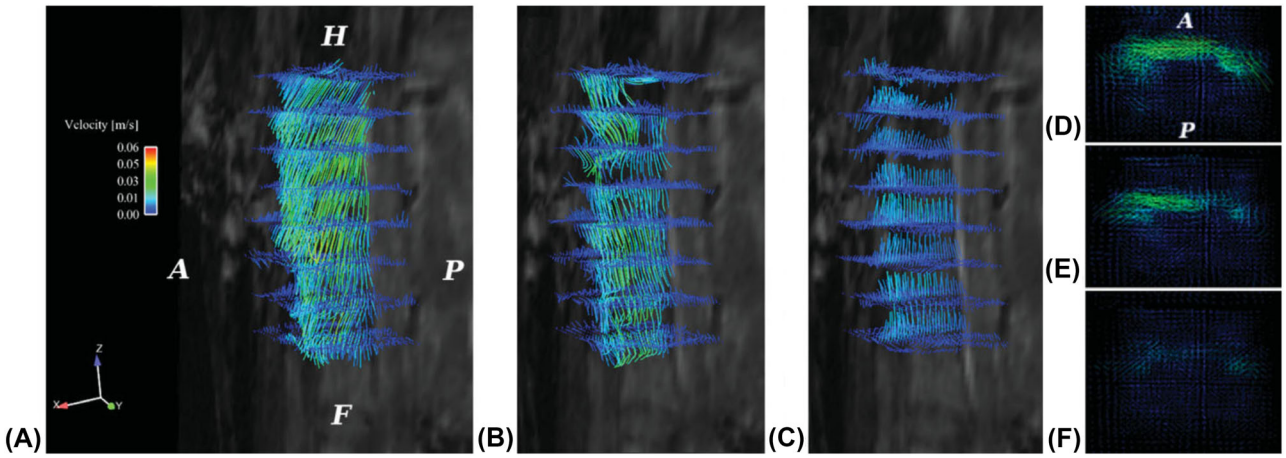

FIGURE 4 Reprinted from Santini et al.[23] Example of four-dimensional cerebrospinal fluid (4D CSF) flow imaging using balanced steady-state free precession (bSSFP) imaging showing streamlines representing CSF flow in the neck (C3–C5 sections) in a healthy volunteer using a V_{enc} of 10 cm/s. Eight planes were placed axially 5 mm apart from each other and were chosen as emitters for the streamlines. Image view is oblique sagittal/coronal approximately 45° in (A–C) The left/posterior direction, and (D–F) Axial. Anteroposterior and head–feet directions are represented by the letters A–P and H–F, respectively. The vectors represent magnitude and direction of velocities of each point at three different cardiac phases: (A and D) Second phase after R wave, (B and E) Third phase, and (C and F) last (eighth) phase. Non-negligible in-plane components are visible in the oblique view.

violating the need for first-order-moment nulling.[100] The authors of that study indicated that, despite the high SNR, the bSSFP sequence implementation may not be ideally suited for the study of vascular hemodynamics, especially when high temporal resolutions are desirable. Other potential limitations of bSSFP 4D CSF flow may include increased susceptibility to field inhomogeneity from longer TRs, which causes phase dispersion and image banding artifacts.

2.1.2 | Low velocities associated with CSF motion

4D CSF flow data acquisition times are frequently extended because of the low velocities associated with CSF motion. Velocities observed across typical CSF ROIs including the CA, foramen magnum (FM), and across vertebrae levels in healthy humans, are usually in the range of 5–20 cm/s.[27,104] However, slower flows are expected in regions such as SAS (<1 cm/s)[105] and PVS (~0.1 mm/s),[106] which are of high interest for studies on brain metabolite clearance.[105,107,108] By contrast, cerebral venous and arterial blood flow velocities are considerably higher (20–100 cm/s).[109,110] The low velocities of CSF can lead to longer acquisition times by extending the duration of the velocity-encoding gradients, which are often run at maximum gradient amplitude. Alternatively, high performance gradient systems with increased amplitude and slew rate could be used; however, these can raise issues related to peripheral nerve stimulation or are limited to head-only MR systems.[111]

Velocity encoding in 4D flow MRI is based on the observation that changes in the MR signal phase along a magnetic field gradient are directly related to the flow velocity.[53–55] Velocity encoding is typically performed using bipolar gradients. By applying a set of bipolar gradients no net phase is accumulated by stationary spins; however, moving spins experience a velocity-dependent phase change, which is proportional to the amplitude and timing of the gradient.[54] During a 4D flow acquisition, the user needs to define an upper velocity limit, the velocity sensitivity encoding parameter, V_{enc}. V_{enc} is the maximum velocity (positive or negative) that can be detected without aliasing occurring. In such a scenario, either the scan needs to be repeated with an increased V_{enc}, or antialiasing correction[112] needs to be performed to ensure the correct velocities are quantified. If V_{enc} is far below the peak velocities, aliasing correction will probably fail. Hence, V_{enc} selection is a crucial choice and may differ largely between patients and controls (Table 1), especially in patients with hyperdynamic CSF flow profiles or even blocked CSF flow. Importantly, changes in V_{enc} correspond to changing the strengths and duration of the velocity-encoding gradients, where the encoding of lower velocities (i.e., a lower V_{enc}) requires larger bipolar gradient areas, leading to longer TEs and TRs. Velocity noise in 4D flow is directly proportional to the V_{enc} and inversely related to SNR in the corresponding magnitude images ($V_{noise} \sim V_{enc}/SNR$).[54,55] This property indicates that the user should balance the choice of V_{enc} between high (to avoid aliasing) and low (for optimal noise performance). Therefore, the optimal V_{enc} is a tradeoff between the minimum detectable velocity sensitivity needed to avoid aliasing. Because of low velocities and longer T1, 4D CSF flow imaging acquisitions will have longer TRs compared with 4D flow imaging of blood. Figure 5 shows an example of bipolar gradient waveforms designed on a 3.0-T system ($S_{max} = 200$ T/m/s, $G_{max} = 80$ mT/m) using 4D flow acquisitions with different prescribed V_{enc} settings. Bipolar gradients designed for a prescribed V_{enc} of 1 cm/s (e.g., SAS CSF) required a much longer time to be played out compared with those for a V_{enc} of 100 cm/s acquisition

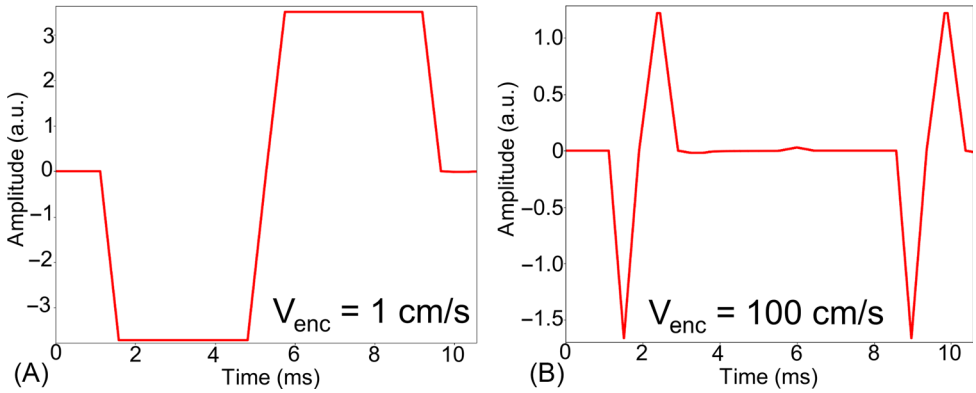

FIGURE 5 Example of bipolar gradients designed in a 3.0-T magnetic resonance imaging (MRI) system with G_{max} = 80 mT/m and S_{max} = 200 T/m/s. Bipolar gradients were designed for a four-dimensional (4D) flow acquisition with different prescribed velocity-encoding (V_{enc}) parameters including (A) 1 cm/s and (B) 100 cm/s representing velocity sensitivities for cerebrospinal fluid and arterial blood flow, respectively. This example demonstrates the longer time required by the system to generate a gradient waveform to encode low velocities compared with high velocities, extending acquisition times.

(e.g., CBF). This example highlights one of the challenges of low V_{enc} 4D CSF flow MRI in current clinical MRI systems. It should be noted that a V_{enc} of 1 cm/s is on the very low end of current CSF flow applications, as most studies use V_{enc} between 5 and 20 cm/s.

Prescription of a low V_{enc} setting in a 4D CSF flow acquisition leads to larger first gradient moments and gradient amplitudes that are associated with rapidly changing magnetic fields. In turn, rapidly changing magnetic fields can lead to phase offsets in the velocity images from induced eddy currents. MRI systems use pre-emphasis to compensate for eddy current effects by purposefully distorting the gradient input waveform. However, eddy current offsets can persist, leading to unwanted phase offset errors that can hinder the reproducibility and accuracy of 4D CSF flow measurements.[39,113,114] These errors can be corrected during the postprocessing of 4D flow images by subtraction of a polynomial fitted to the static tissue background. There exist various implementations of polynomial fitting algorithms, including local and whole brain polynomial fitting, for background offset correction. These approaches have been demonstrated to correct 4D CSF flow phase offsets in regions such as the CA, improving the quality of the estimated velocity fields (Figure 6).[39,115] Because CSF net flow rates are typically small, uncorrected phase offset errors may lead to false interpretation of the direction of CSF flow in compartments that are central to understanding normal and pathological CSF physiology (e.g., the CA[39]). More recently, machine learning implementations have demonstrated the capability to remove background field offsets in neurovascular 4D flow MRI,[81] something that could be extended to 4D CSF flow.

To allow clinically feasible 4D CSF flow scan times, fast data acquisition schemes are necessary. 4D flow MRI data acquisition methods have largely employed Cartesian readouts. Cartesian readouts allow for fast and efficient image reconstruction, and structured artifacts (e.g., fold-over) can be tolerable to a limit; however, the sampling trajectory is relatively slow as k-space is filled line-by-line. To accelerate Cartesian readouts, partial Fourier techniques and EPI[116] acquisitions can be utilized. Alternatively, reduced 4D flow MRI scan time can be achieved using non-Cartesian readout trajectories, such as stack of radials,[117] 3D radial,[76,118] and spirals.[119] Each readout trajectory carries tradeoffs that must be carefully considered when developing a 4D CSF flow protocol. For example, fast EPI readouts can help reduce the long scan times associated with 4D flow; however, they can be sensitive to displacement and resolution artifacts from the time between velocity encoding to TE and phase accumulation contributions from the motion-sensitive readout strategy.[116,120] This has been observed in MRI simulations and in in vitro experiments using realistic imaging parameters, where EPI-based 4D flow with longer TE resulted in considerable velocity misregistration and spatially varying degradation of resolution.[116] That study showed EPI readouts can lead to spatially varying broadening of the point spread function, indicating that, while faster, EPI readouts can be challenging for 4D flow MRI.

Spiral readout trajectories are promising for fast 4D CSF flow imaging. Spiral trajectories allow for gains in SNR from efficient data collection[121] and can be used to reduce scan times. Further reductions on scan time can be achieved with flexible undersampling during spiral readout design, although this is not unique to spiral readouts. Center-out spirals have short TEs, improving robustness against bulk motion and susceptibility dephasing.[122] One of the main limitations of widespread clinical adoption of spiral readouts is their sensitivity to B0 off-resonance, gradient imperfections, and susceptibility effects. These can lead to highly disruptive artifacts, which are proportional to the readout duration. In cardiac and aortic imaging studies, spiral 4D flow has led to significantly faster scans with 2- to 3-fold scan time reductions compared with SENSE-accelerated Cartesian scans.[119,123] In those studies, there were no significant reductions in data quality from streamline analysis and cardiac output measures between spiral and Cartesian acquisitions.

Figure 7 shows an example of 4D CSF flow magnitude data from a healthy volunteer acquired using spiral and Cartesian readouts. The data were acquired using the same imaging parameters (V_{enc} = 7.5 cm/s); however, improved image sharpness was achieved in the spiral (Figure 7B) compared with the Cartesian (Figure 7A) scan because of the more efficient sampling of k-space. This result is important, as CSF flow in small

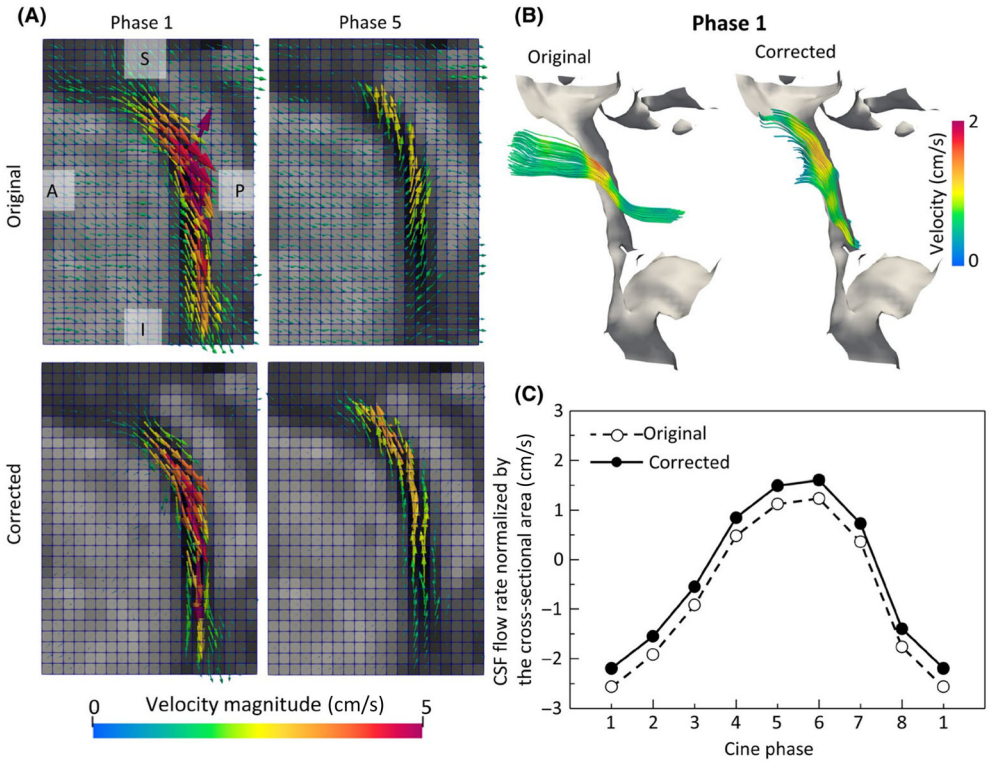

FIGURE 6 Reprinted from Yavuz et al.[39] Snapshots of velocity distribution in the cerebral aqueduct (CA) in the sagittal plane on the original four-dimensional flow magnetic resonance imaging (4D flow MRI) images (A, top) and images corrected for eddy current phase offset error and aliasing artifacts (A, bottom), streamlines in the CA in the original (B, left) and corrected (B, right) velocity maps, and rates of cerebrospinal fluid (CSF) flow through the CA derived from the original and corrected velocity maps (C). The eddy current phase offset errors were expressed as a second-order polynomial function using a whole background correction approach combined with robust regression. The 4D CSF flow data were acquired in a normal pressure hydrocephalus patient using a V_{enc} of 5 cm/s.

ROIs is of high interest (e.g., SAS, PVS), and image blurring and partial volume effects can lead to inaccurate flow quantitation. The fully sampled spiral scan time was 6 min, compared with 10 min for a highly accelerated Cartesian scan (i.e., 8× GE Hyperkat [Kat-ARC]). Using spirals, 4D CSF flow signal preparation can be further exploited to boost SNR by designing trajectories with longer readouts. However, spiral readout lengths need to be optimized to balance SNR gains with increased image artifacts and T2* decay effects. Figure 7B,C show an example of identical spiral 4D CSF flow scans with different readout lengths (3.5 [B] vs. 13.5 [C] ms). In the longer readout scan, SNR gains were undermined by high levels of image blurring from B0 off-resonances and air/tissue interphase susceptibility artifacts. Substantial progress has been made in methodology for spiral off-resonance correction. For example, using expanded signal models, researchers have demonstrated spiral image corrections for off-resonance and magnetic field dynamics using data recorded during the image acquisition with NMR field probes.[124] Figure 8 shows an example of two spiral trajectories designed for low and high V_{enc} scans. In this case, the 4D CSF flow scan corresponds to the low V_{enc} trajectory with optimized readout to improve SNR.

Three-dimensional radial readouts can also be used for fast 4D CSF flow imaging. Center-out radials have short TEs and are inherently less sensitive to motion. Bulk motion during radial readouts leads to image blurring and noise-like artifacts, rather than the coherent ghosting seen in Cartesian images.[125] Exploiting variable density 3D radial undersampling,[76,117,126] high SNR images with large volumetric coverage and high spatiotemporal resolutions can be achieved for neurovascular 4D flow imaging.[67,68,88,89,110] In radial readouts, oversampling of the center of k-space and reasonable undersampling of higher k-space frequencies results in benign streak artifacts, and can be utilized for self-navigation and bulk motion correction.[127,128] Recently, 3D-radials have been used for rigid head motion correction in neurovascular 4D flow of geriatric populations.[129,130] The utilization of radials for 4D CSF flow imaging has been considerably less studied. Figure 9 shows an example of magnitude and velocity images derived from 4D CSF flow data in a healthy volunteer using spiral (A) and radial (B) readouts. Radial images appear less noisy than spiral images; however, small structures such as vessels and the CA are sharper in spiral images. The noticeable blurring in radial images is probably a result of the lower efficiency of radials to sample higher frequencies of k-space. Blurring of small structures can lead to partial volume effects on quantitative measures derived from 4D CSF flow, as shown in cardiac-resolved data from five healthy volunteers (Figure 9C). Further, cardiac-resolved 4D CSF flow profiles in the CA depict sharp systolic and diastolic phases on spiral images; by comparison, flow profiles from radial images display less structured and damped features, probably as a result of partial volume effects. 2D PC approaches are still the most suitable when accurate estimation of peak flow is desirable, given the lower spatiotemporal resolution associated with 4D flow methods.

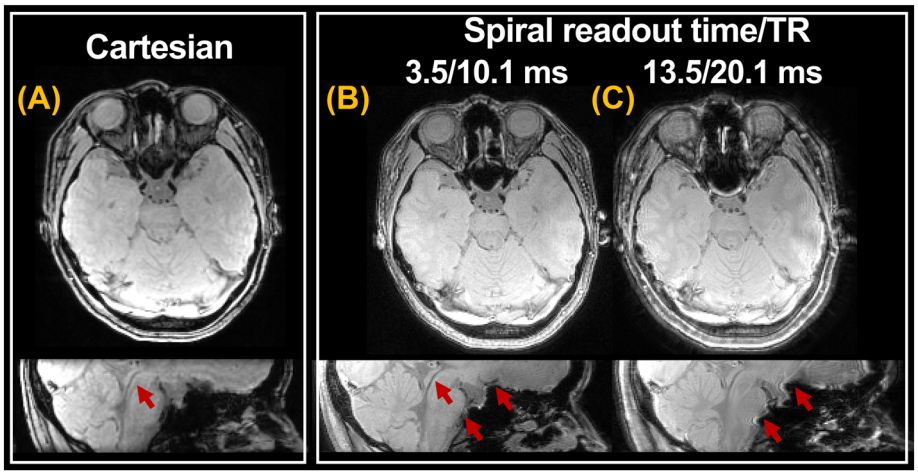

FIGURE 7 Example of four-dimensional cerebrospinal fluid (4D CSF) flow magnitude images using (A) Cartesian, and (B and C) Spiral readouts. Images were acquired with 1-mm isotropic spatial resolution, imaging volume of 25.6 × 25.6 × 7 cm^3, TR/TE = 10.1/5.7 ms (Cartesian [A]) and 10.1/3.5 ms (spiral [B]), flip angle = 4°, V_{enc} = 7.5 cm/s and scan times of 10 min (Cartesian after GE Hyperkat [Kat-ARC] acceleration factor 8) and 6 min (spiral no acceleration). Higher image sharpness was observable in (B) Spiral images compared with (A) Cartesian, which benefited delineation of the cerebral aqueduct (red arrow). Overall, greater image quality was attainable in 4D CSF flow imaging using spirals compared with Cartesian readouts at considerably shorter scan times (6 vs. 10 min). One way to increase signal-to-noise ratio (SNR) in 4D CSF flow imaging is to acquire more data during the spiral readout. In (C), Spiral images were acquired with similar parameters as in (B) (except flip angle [Ernst angle]); however, dataset (C) was acquired with 8 × oversampling of the center of k-space, leading to longer readout time. Data collected with longer readouts (13.5 ms) displayed higher SNR but more off-resonance and susceptibility artifacts (blurring) (red arrows), compared with data with shorter readouts (3.5 ms). Robust strategies to minimize these off-resonance and susceptibility artifacts can further increase the value of spiral imaging.

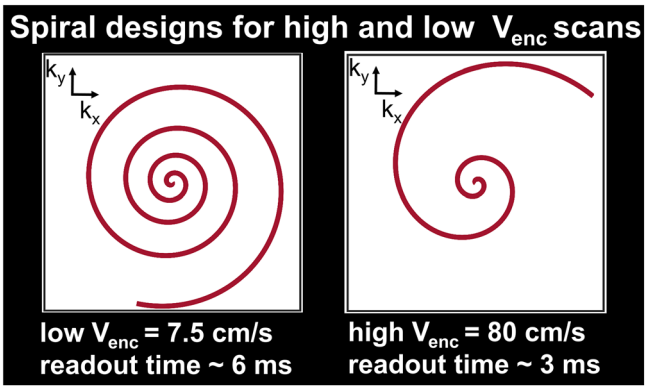

FIGURE 8 Example of spiral readout trajectories designed for low (left panel) and high (right panel) velocity-encoded (V_{enc}) four-dimensional flow scans. For the low V_{enc} scan (7.5 cm/s), longer readout time with spirals can be leveraged for more efficient k-space data sampling and boost in signal-to-noise ratio. Shorter spiral readouts were designed for the high V_{enc} (80 cm/s) scan to reduce signal loss from inflow effects, which are less of a concern in the low V_{enc} scan.

In summary, 4D CSF flow MRI scan times can be significantly reduced using accelerated Cartesian and non-Cartesian trajectories. Considerations for trajectory design must include k-space sampling efficiency and robustness to eddy currents, susceptibility artifacts, and system imperfections. Finally, to determine which trajectories are best suited for accelerated 4D CSF flow applications, side-by-side evaluations of accuracy are warranted.

2.1.3 | Cardiac and respiratory gating

Characterization of CSF dynamics is important to study normal physiology, pathophysiology, and CSF-mediated pathways such as proposed models of brain clearance. Studies using 2D PC MRI have quantified CSF motion contributions from both cardiac and respiratory cycles, which can vary across anatomical ROIs.[131,132] Currently, real-time 2D PC MRI approaches can provide simultaneous evaluation of cardiac- and

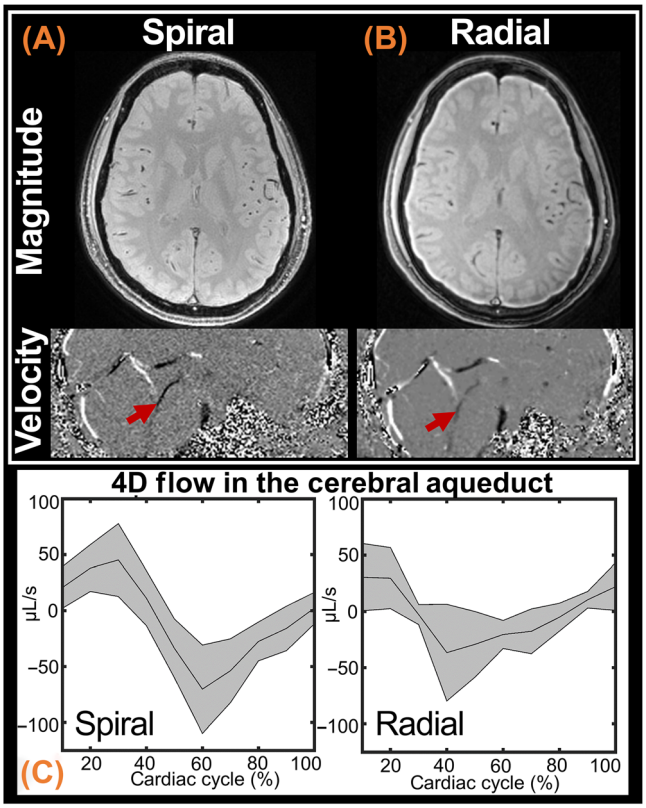

FIGURE 9 Magnitude and velocity data derived from four-dimensional cerebrospinal fluid flow magnetic resonance imaging (4D CSF flow MRI) acquired using (A) Spiral, and (B) Radial readouts. Overall, spiral images depict higher image sharpness compared with more blurred radial images. Noise levels appear to be lower on the radial images. Higher sharpness in spiral images indicates better sampling efficiency, compared with radial images generated from oversampling of the center of k-space while undersampling the edges. Some off-resonance effects are noticeable in the anterior aspect of the brain in the spiral images. (C) Average CSF flow profiles across five healthy volunteers in the cerebral aqueduct from retrospective cardiac binning of 4D CSF flow data acquired using spiral and radial readouts. Flow profiles from spiral 4D CSF flow images depict sharp flow changes from systolic and diastolic cardiac phases, compared with dampened flow profiles from radial images that are probably affected by blurring artifacts from the less efficient k-space sampling of radial readouts.

respiratory-driven CSF flow.[75,133,134] Leveraging rapid imaging, real-time methods allow for continuous data acquisition without relying on any gating, synchronization, or repetition of the underlying movement or contrast dynamics. We can also use 4D flow MRI to study CSF motion, its driving forces, and coupling among the various neurofluids (Figure 10). However, gating of 4D CSF flow data can also extend scan times to meet adequate temporal resolution for cardiac- and respiratory-resolved imaging. As data are distributed among temporal phases, SNR challenges for 4D CSF flow imaging can be exacerbated and undersampling artifacts increased. Time-resolved 4D flow data are either prospectively or retrospectively sorted across temporal bins using cardiac and respiratory triggers acquired during the MRI scan. Respiratory trigger data are typically collected using respiratory belts placed on the subject's diaphragm or abdomen. Cardiac triggers are recorded using ECG gating or peripheral pulse gating (PPG). PPG is less invasive and relies on an MRI-compatible photoplethysmogram worn on the subject's finger during the MRI examination, leading to reduced patient burden and preparation time. PPG is also less susceptible to electromagnetic interference compared with ECG. Recent studies have shown that, for CSF flow quantitation at the level of the spine (e.g., cervical spine), using PPG can provide reasonable results over cohorts of at least five subjects compared with results using ECG gating.[135] However, PPG cardiac waveforms are broad and can be variable in rise time compared with ECG triggering from very narrow R-waves. PPG gating is also more susceptible to timing issues, because it is unclear when the R wave appears in the finger versus head, especially for patients versus healthy, and women versus men, which could lead to missing parts of the cardiac cycle during prospective gating.[136–138] Recent technological advances such as pilot tone, which exploits that a constant radio-frequency can be modulated by physiological motion without physical contact, have shown promise as an alternative to ECG and PPG during 4D flow examinations.[136–138]

Prospective gating is often used by vendors to acquire 4D flow data during a specific acquisition window (e.g., between cardiac trigger R-waves). Data acquisition begins after detection of a desired physiologic event (e.g., R wave) and continues until the desired temporal phases have been captured. For cranial and spinal 4D CSF flow, prospective gating at high spatiotemporal resolutions can lead to long scan times. Prospective gating limits the dynamics that can be resolved (e.g., cardiac, or respiratory). Alternatively, retrospective gating collects data continuously

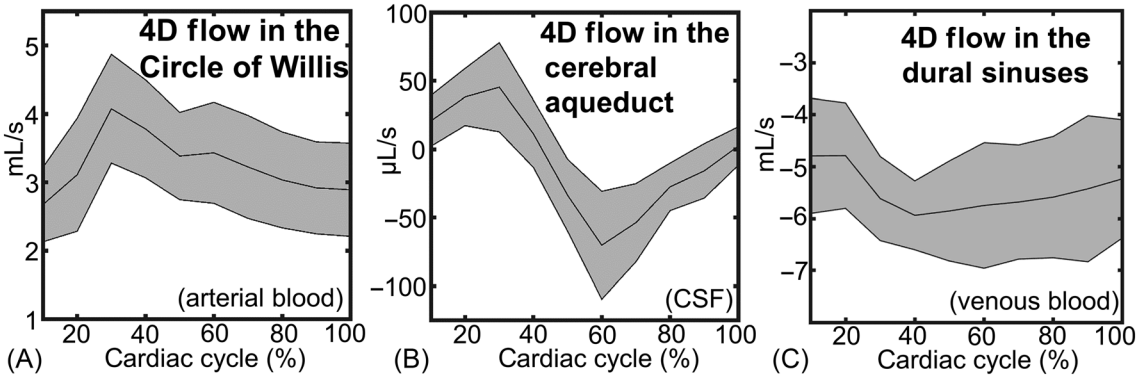

FIGURE 10 Example of cardiac-resolved flow profiles of (A) Blood in the Circle of Willis (internal carotids), (B) Cerebrospinal fluid (CSF) in the cerebral aqueduct, and (C) Venous blood in the dural venous sinuses derived from four-dimensional flow magnetic resonance imaging (4D flow MRI) data using velocity-encoding parameters of 80 cm/s (blood) and 7.5 cm/s (CSF). Data were acquired in five healthy volunteers using spiral readouts and retrospectively reconstructed the cardiac cycle with 10 temporal phases. These data can be used for studying neurofluids coupling because of arterial pressure-induced CSF flow dynamics.

followed by reordering and grouping according to the phase of the cardiorespiratory cycle using trigger data. This allows for higher SNR and retrospective binning of the cycle of interest. In cardiac and carotid 4D flow imaging applications, retrospective gating has been demonstrated to increase temporal resolution, allowing the detection of hemodynamic features (e.g., retrograde flow) not observable with lower temporal resolution from prospective gating.[123,139] In retrospective gating, sufficient randomized sampling of the center of k-space is wanted for reconstruction of the temporal phases, which can be challenging to achieve using Cartesian readouts. Retrospective gating of data acquired using non-Cartesian readouts can be practical as trajectories are more flexible, and because oversampling of k-space (e.g., center-out radials) enables view sharing to reduce undersampling artifacts across temporal phases in 4D flow.[140,141] Retrospective gating can also allow for theoretical temporal resolutions of less than 1 TR in neurovascular 4D flow with appropriate reconstruction support (e.g., low rank).[80] Overall, either prospective or retrospective gating strategies can be used for 4D CSF flow imaging. However, the reconstruction flexibility enabled by retrospective gating allows for higher temporal resolutions, multidynamics reconstruction, and higher SNR.

2.2 | Current approaches to facilitate 4D CSF flow MRI

Researchers have used compressed sensing reconstructions to reduce the scan time of 4D CSF flow.[37] In a study that combined compressed sensing and parallel imaging, a 40% scan time reduction was achieved while maintaining clinical utility and enabling an ~6 min acquisition for the cervical spine and ~14 min for coverage of the entire spinal cord (Figure 11).

Multi-V_{enc} approaches can also be used to reduce 4D flow scan time when targeting both blood and CSF. A 12.5% scan time reduction can be achieved by sharing a reference scan between the high and low V_{enc} acquisitions.[77] More recently, ~35% scan time reductions in neurovascular dual-V_{enc} 4D flow scans were demonstrated by undersampling of the high V_{enc} acquisition while preserving the dynamic range and VNRs of dual-V_{enc}.[78] Other studies have demonstrated the feasibility of accelerating neurovascular 4D flow acquisitions by 25% using machine learning and a convolutional neural network (CNN) that produces three directional velocities from three flow encodings, without requiring a fourth reference scan measuring background phase.[81] The authors used neurovascular 4D flow scans to train a CNN using supervised learning. The produced three-point velocities showed excellent agreement with the velocities derived from standard reconstruction using all four flow encodings with ~1.5% errors in the velocity values, and correlations as high as 0.992. The authors noted that the performance of the neural network depended on the loss function used for training, with improved performance when velocities across the spectrum were evenly weighted in the loss function, hence increasing the weight of vessels compared with static background tissue. Machine learning approaches can also be combined with CFD to reduce error in accelerated 4D flow MRI.[142–144] Researchers have augmented 4D flow MRI data with CFD-informed CNNs to produce enhanced physiological flow fields.[145] Using high-resolution patient-specific CFD data, they trained a CNN that was subsequently used to enhance MRI-derived cerebrovascular velocity fields. In simulated images, phantom data, and in vivo human subject data, the trained network successfully denoised flow images and decreased velocity error, particularly near vessel walls. CNNs have also been shown to map the nonlinear relationship between fine- and coarse-scale velocity fields in 4D flow, allowing for a 4-fold increase in spatial resolution of the velocity field.[146] Overall, while these approaches were demonstrated for blood flow imaging, they could be adapted for CSF flow imaging, leading to reduced scan times from collection of fewer velocity encodes, denoised velocity fields, and high spatial resolution images generated from lower spatial resolution scans.

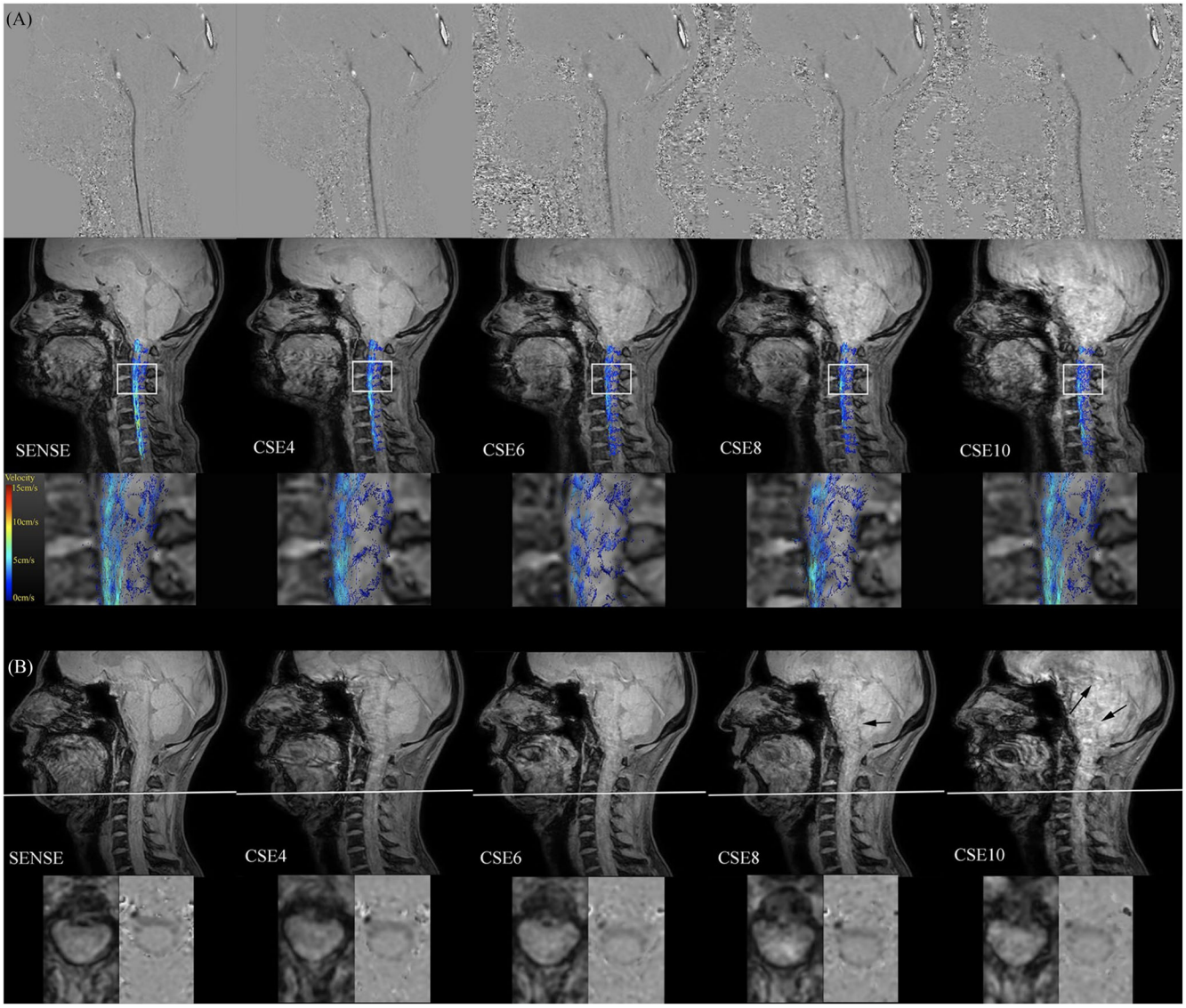

FIGURE 11 Reprinted from Jaeger et al.[37] (A) Phase and pathline images, and (B) Magnitude images for different compressed sensing acceleration factors. Imaging artifacts are highlighted with black arrows in compressed sensitivity encoding (CSE) 8 and CSE10.

Most 2D PC and 4D flow MRI studies have measured CSF dynamics in large ROIs such as the ventricles, the spinal SAS, and the CA. However, to further inform on normal CSF physiology and the role of CSF dynamics in brain clearance, simultaneous assessment of CSF flow in multiple small ROIs is necessary. For instance, a thorough description of the CSF circulation (including production and reabsorption) would require simultaneous assessment of CSF dynamics in the ventricles and the entire SAS. Further, a comprehensive understanding of CSF dynamics linked to brain clearance would require mapping cardiac and respiratory contributions in both SAS and PVS compartments. Such potential 4D CSF flow applications would demand high spatiotemporal resolution as ROIs are small and velocities are low. Leveraging high field strengths (i.e., 7.0 T) and using pulse-gradient-spin-echo (PGSE) EPI, researchers have demonstrated high spatiotemporal resolutions with flexibility for V_{enc}, robustness to physiological artifacts (e.g., breathing-related B0 field variation), and high acquisition efficiency in 4D CSF flow MRI (Figure 12).[105] PGSE EPI for 4D CSF flow allowed flexibility to achieve low V_{enc} from a long velocity-encoding time and strong T2 weighting from long TEs, reducing signal from blood for improved specificity to CSF. This approach has enabled cardiac pulsation and respiration-driven CSF flow dynamics in the ventricles and SAS. Using this technique, researchers observed that cardiac pulsation led to stronger and faster CSF flow changes than respiration in most ROIs (Figure 12). Theoretical and experimental data at high field strengths (i.e., 4.7 and 7.0 T) have shown limits of flow detection as low as 1 μm/s using PC techniques.[147,148] To put such velocity into perspective, in clinical 3.0-T MRI systems, a V_{enc} of 1 cm/s can be challenging to prescribe.

Another key technology is high performance gradient systems that can allow for faster data collection and increased velocity sensitivity in 4D CSF flow MRI. The new generation of high performance gradient systems in head-only MRI scanners can achieve 3–4-fold improvements in

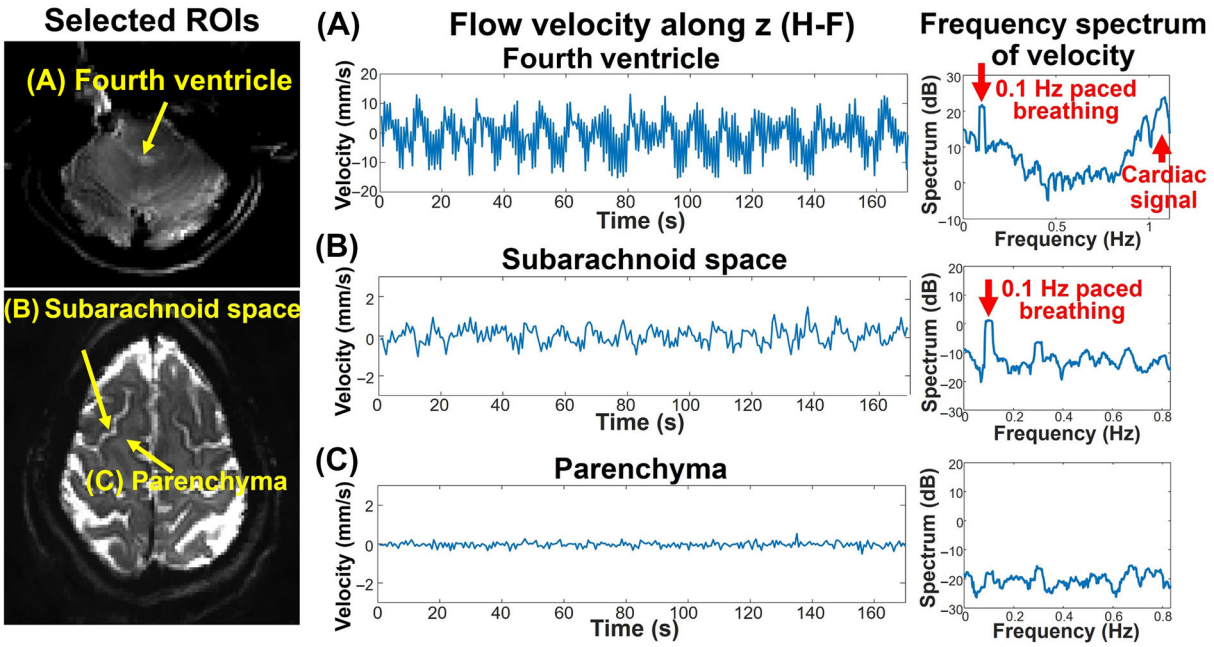

FIGURE 12 Figure courtesy of Dr. Zijing Dong, Massachusetts General Hospital.[105] Four-dimensional cerebrospinal fluid (4D CSF) flow at 7.0 T using pulse-gradient-spin-echo echo planar imaging. Respiration-associated periodic CSF velocity changes were observed in both the (A) Fourth ventricle with an amplitude of ~10 mm/s, and in (B) Subarachnoid space with ~1 mm/s. The frequency spectra showed high energy at 0.1 Hz, corresponding to the frequency of the paced breathing. (C) This feature was not detected in a region of interest within the parenchyma. In addition to respiration, strong modulation from cardiac pulsation also appears in the time series as rapid peaks riding on the slower, periodic respiratory waveform.

gradient strength and slew rates, enabling reduced minimum TR and TE, shortening the velocity-encoding time and reducing to artifacts.[111] Preliminary studies have demonstrated the feasibility of performing cardiac-resolved PC MRI with ultralow $V_{enc} = 0.24$ mm/s (using spin echo) to depict very slow intracerebral coherent motion of the order of 0.1 mm/s in humans (Figure 13). Such velocity sensitivity is enabling research studies of glymphatics and IPAD clearance models, and sleep versus wakefulness CSF motion variability.[106]

2.3 | 4D CSF flow markers and applications

2.3.1 | Derivable markers of 4D CSF flow

While postprocessing solutions for 4D flow MRI are both commercially[149] available (e.g., cvi42 [Circle Cardiovascular Imaging] and GTFlow [GyroTools]) and open sourced,[85,112] these have largely been tested on the processing of blood flow imaging datasets. Such tools include algorithms for the correction of background phase offsets, antialiasing, vessel segmentation, and derivation of hemodynamic parameters. However, these approaches need to be evaluated for 4D CSF flow imaging and new algorithms will probably need to be incorporated to facilitate segmentation of complex CSF conduits from 4D CSF flow data. Currently, 4D CSF flow postprocessing is frequently performed using in-house code, which can hinder reproducibility when it is not open source. Below, we describe a series of 4D CSF flow markers currently being utilized and developed by the scientific community.

Velocity field mapping using 4D flow MRI enables the derivation of many fluid dynamic-related imaging markers. Various 4D flow-based hemodynamic markers have found great clinical and research utility in cardiovascular[63] and cerebrovascular[67–69] applications. However, the utility of many potential 4D CSF flow markers is less established and is an active research area. Further, reference data on healthy volunteers are almost nonexistent, and need to be established to compare with suspected pathologies. Here, we summarize basic and more advanced proposed 4D CSF flow imaging markers (Table 1). Notice that all 4D CSF flow studies were cardiac gated, highlighting the lack of respiratory-gated 4D CSF imaging studies.

4D CSF net flow rates,[37,39] reversed flow,[39] and mean velocities (MVs)[26,34,35] have typically been assessed in large ROIs such as the CA,[5,35,39] spinal canal,[37] FMa,[5] ventricles[26,34,35] (lateral, third, and fourth), and the foramen of Monro (FMo).[26,35] Others have assessed systolic and diastolic flow rates separately in the FM and spinal canal,[12] as flow rates often averaged to near zero across the cardiac cycle. Hence, many

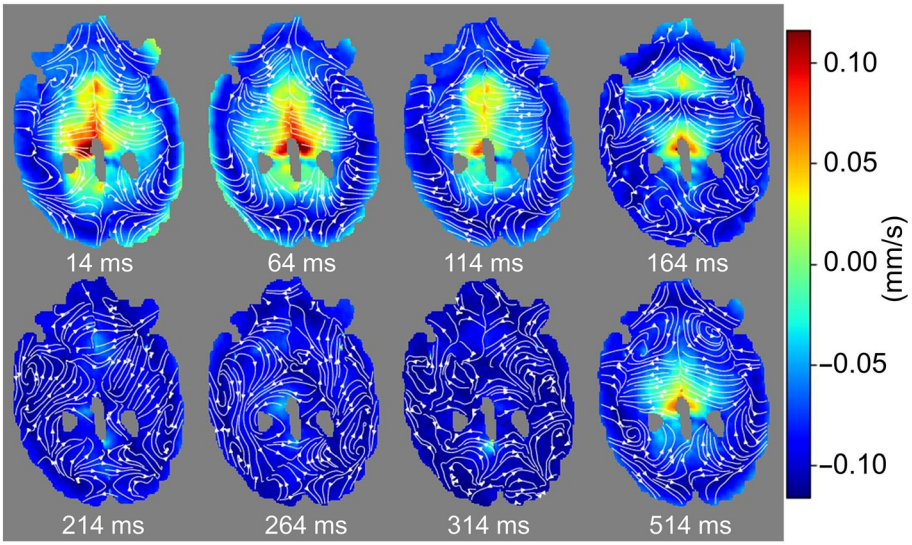

FIGURE 13 Figure courtesy of Dr. Thomas K. Foo, GE Global Research.[111] Example of velocity images from data acquired at 3.0 T using the MAGNUS gradient system at $G_{max} = 200$ mT/m and $S_{max} = 500$ T/m/s and a very low V_{enc} of 0.24 mm/s. The vector lines show brain and cerebrospinal fluid (CSF) motion depicted across the cardiac cycle. High performance gradient systems allow phase contrast magnetic resonance imaging at very low V_{enc} enabling the study of tissue and CSF motion coupling, and brain clearance models.

studies have not assessed cardiac-averaged flows, but focused on PSV or peak diastolic velocity (PDV) alone (i.e., the highest systolic and diastolic flow rates; in opposite directions), an approach that has been used in the FM/spinal canal,[10,12,24,30,31] but also in ventricular (including CA and FMo) ROIs.[35] SV, that is, the net flow over a cardiac cycle, has also been assessed in the FM/spinal canal,[27] and in the foramens and cisterns,[5] and flow magnitude (direction and cardiac-averaged) has also been computed voxel-wise to define a binary 3D ROI of significant flow connectivity for semiautomatic identification of CSF occlusions[25] (or near-occlusions).

Streamlines derived directly from the velocity fields have been used to visualize flow patterns in the FM/spinal canal[12,23,24] and in the CA, cisterns, and foramens,[5,38] providing visually available information regarding the quality of the 4D flow, and allowing for potential visualization of physiological and pathophysiological flow patterns. Pressure gradients,[28,29,33,34] rotation,[33] and acceleration (velocity-derivative) fields[34] have also been used to assess pathological CSF flow patterns associated with CMI,[28] INPH, and AD,[33] and to understand the role of CP in physiological conditions.[34]

Wall shear stress (WSS),[5] oscillatory shear stress (OSS), and the oscillatory shear index (OSI),[38] have also been proposed in 4D CSF flow studies. While WSS is the product of an assumed fluid viscosity and the velocity derivative with respect to distance from the vessel wall, OSS was defined by calculating the shear stress at each point of the cardiac cycle with a sign function related to the direction of the cardiac-resolved WSS in relation to the cardiac-averaged WSS. The OSI was designed to monitor the number of direction changes of the WSS during one cardiac cycle.[38] It should be highlighted that the reproducibility of 4D CSF flow markers in general, but in particular of parameters like WSS that demand high spatial resolution, needs to be demonstrated systematically to provide a better indication of their potential clinical and/or research utility.

Finally, because quantifying net flows (cardiac-averaged) and their direction is challenging in low-flow regions of the SAS, one study used a correlation-mapping and time delay-mapping approach,[36] suggesting that the differences observed in the delay time of CSF wave propagation could potentially inform on CSF dynamics disturbances linked to aging and INPH.[36]

2.3.2 | Idiopathic normal pressure hydrocephalus

INPH is a neurological disorder characterized by dilation of the cerebral ventricles. The condition typically occurs in the elderly (average onset at age 70 years[150]), with clinical symptoms including gait impairment, urinary incontinence, and cognitive deficits.[150] While the etiology of INPH is not entirely understood, altered CSF absorption rates and flow dynamics probably play a role.[151–153] In contrast to other neurological disorders (e.g., AD), INPH is treatable by inserting a ventriculoperitoneal shunt that diverts excess CSF from the ventricles to the peritoneal cavity, a treatment that often alleviates symptoms and slows disease progression.[150] Whether a patient will benefit from shunting is difficult to determine based on clinical symptoms and ventricular size alone. Tests based on CSF pressure and flow dynamics (e.g., the CSF tap test[150,154] or CSF flow pulsations[151–153]) may provide additional information.

2D PC studies have commonly observed retrograde flow in the CA of INPH patients.[19,155] Some researchers have hypothesized this retrograde flow is driven by a small pressure gradient because of glymphatic dysfunction that forces SAS CSF to the ventricular CSF in INPH.[153] Further, 4D CSF flow studies have found reversed flow rates and higher shear stress (WSS and OSI) in the CA and FMa of INPH patients compared with controls (Figure 14).[5,38] Importantly, 4D CSF flow can be utilized for simultaneous measures of CSF flow pulsatility distribution throughout the cranium including CA (ventricular flow), prepontine cistern (supratentorial SAS), and cervical SAS (intracranial flow). Such assessments are not practical with manual plane prescription from 2D PC methods. From these 4D flow measures, relative distributions could be obtained by estimating ratios (e.g., ventricular to SAS flow). Such ratios have been assessed in the past and have been implicated as a possible cause for ventricular enlargement in hydrocephalus patients.[156,157]

2.3.3 | Chiari I malformation

CMI is defined as downward herniation (≥ 5 mm) of the cerebellar tonsils below the level of the FM. CMI can lead to changes in intracranial volume and pressure, and a variety of symptoms including headache, neck pain, gait instability, paresthesia, dizziness, poor motor coordination, and swallowing difficulties.[158] Current clinical studies support CSF flow and brain motion imaging for clinical decision making in extreme cases of CMI.[158] For example, in cases where the herniated tissue severely restricts CSF flow then surgery is helpful. However, in patients who do not meet the extreme case criteria, an objective test to help decide between conservative and surgical treatment options using CSF flow imaging is currently lacking. 4D CSF flow MRI might help provide noninvasive tests for these milder cases. Indeed, several 4D CSF flow publications have used subject-specific phantoms (based on anatomical MRI scans) to quantify flow in the craniovertebral junction and the spinal canal of CMI patients and healthy controls (Table 1).

Studies using such models have shown good agreement between 2D PC MRI and 4D CSF flow (Figure 15).[10] However, multicenter experiments across five different centers found poor levels of reproducibility of both 2D and 4D CSF flow. Each center tended to have a relative offset based on the specific scanner used, indicating that there might be a need for CSF flow-standardized scanner calibration techniques. Human studies have suggested superior inter-reader agreement in 4D CSF flow compared with 2D PC MRI and a correlation between reduction in PSV and change in syrinx (fluid-filled cyst) size preoperatively and postoperatively.[11] Others that leveraged 4D CSF flow to characterize complex

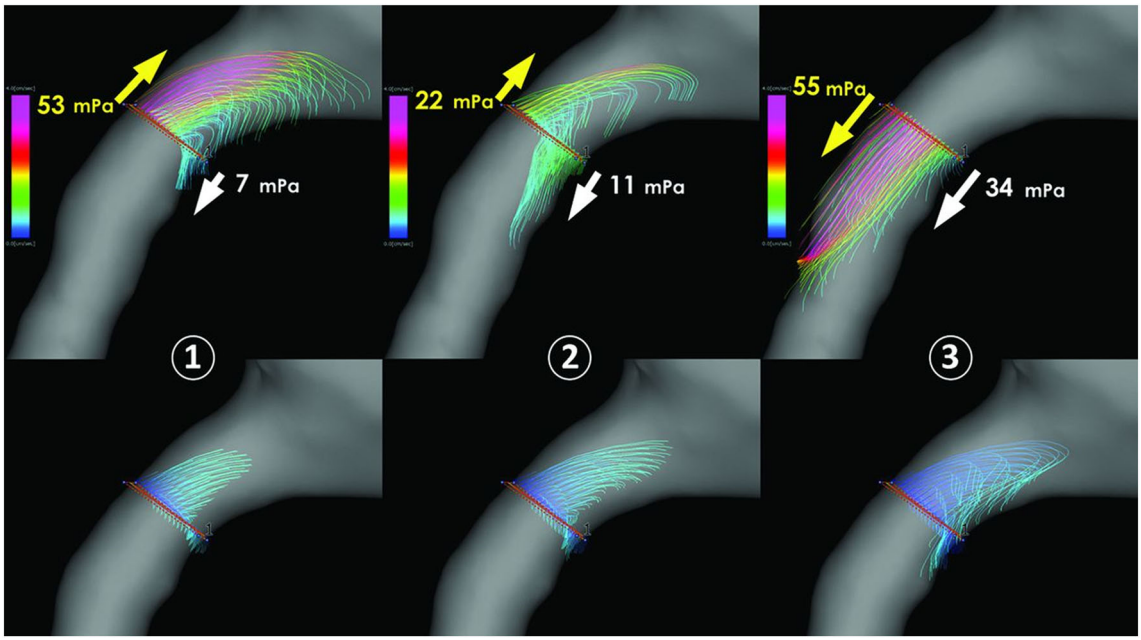

FIGURE 14 Reprinted from Yamada et al.[38] Oscillation of wall shear stress (WSS) due to bidirectional cerebrospinal fluid (CSF) flow through the cerebral aqueduct. The example shows temporal changes of the reciprocating CSF motion during one cardiac cycle in a 77-year-old man diagnosed with idiopathic normal pressure hydrocephalus measured using four-dimensional CSF flow magnetic resonance imaging (4D CSF flow MRI). The colored path lines (lower figures) show the flow as a moving trajectory of the virtual particle through the middle part of the cerebral aqueduct in one heartbeat. The color and length of 3D streamlines (upper figures) indicate the flow velocity as pink for fast and blue for slow. The arrows indicate the WSS vector produced by the flow parallel to the wall surface. The size and direction of the arrows indicate the magnitude and direction of the WSS vector. Temporal changes of the WSS vector at the dorsal region (yellow arrows) were larger than those at the ventral region (white arrows).

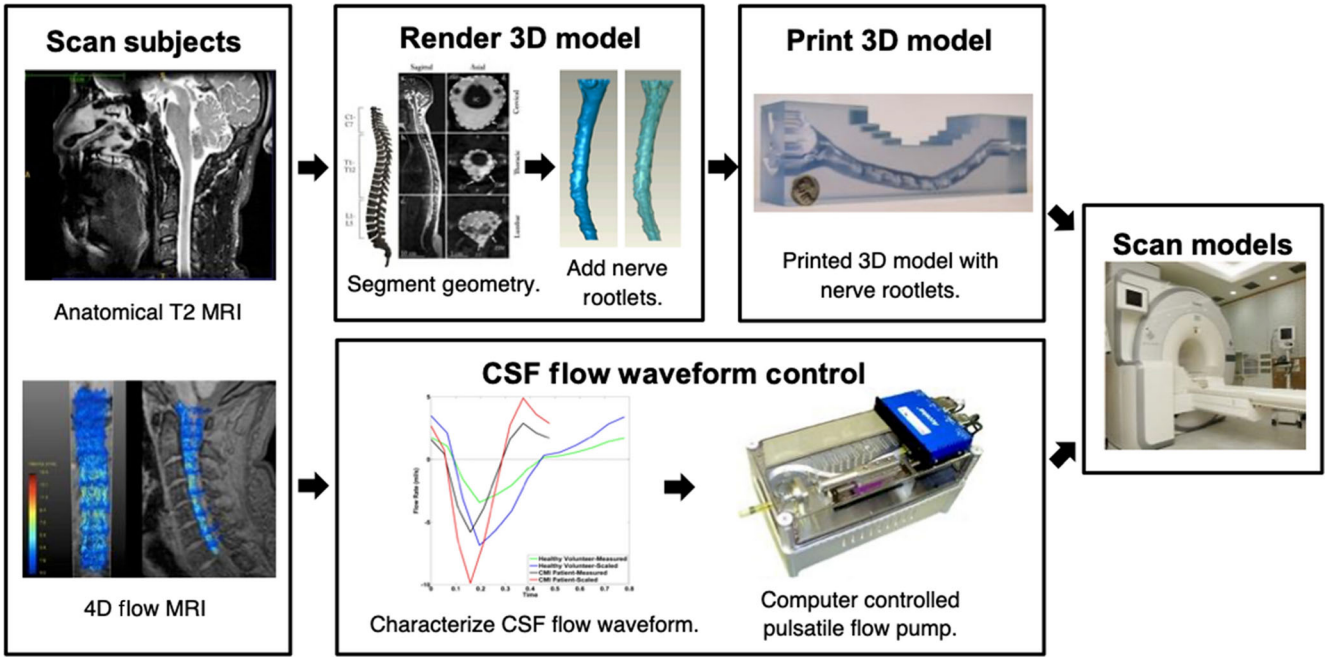

FIGURE 15 Reprinted from Williams et al.[10] Development of in vitro models based on subject-specific scans. First, subjects were scannedusing T2 anatomical magnetic resonance imaging (MRI) and four-dimensional (4D) flow MRI. The anatomical MRI was then used as the basis for the three-dimensional (3D) model. The 4D flow MRI allows the determination of the cerebrospinal fluid (CSF) flow waveform, which informs a computer-controlled pump. The model is then connected to the pump and scanned at each MRI center.

hydrodynamics in CMI patients measured flow abnormalities at the craniocervical junction in the form of heterogeneous flow. Anterolateral flow jets and flow vortex formation were most prevalent in patients with syringomyelia (i.e., with formed syrinx).[12] The authors argued that 4D CSF flow has the potential to improve our understanding of the mechanisms that lead to the formation of syringomyelia.

2.3.4 | Spontaneous intracranial hypotension

Another disorder for which diagnosis could benefit from 4D flow imaging is SIH. SIH is characterized by low ICP and is frequently caused by spinal CSF leaks that might lead to an orthostatic headache syndrome.[60] While no records of 4D CSF flow studies in SIH were found, recently published data support 2D PC MRI of CSF flow as a promising diagnostic tool in SIH. In that study, patients with SIH presenting with spinal longitudinal extradural fluid collection showed higher CSF flow and higher spinal cord motion at the upper cervical spine.[60] The authors hypothesized that the increased craniocaudal motion of the spinal cord might produce increased mechanical strain on neural tissue and adherent structures, leading to cranial nerve dysfunction, neck pain, and stiffness in SIH. Importantly, 4D CSF flow could enhance 2D PC studies of SIH by allowing full coverage of the spinal cord and the upper cervical spine, instead of selective landmarks (e.g., C2/C3 and C5/C6), providing further insights into the pathophysiology of SIH.

2.3.5 | Brain clearance

CSF-mediated brain-clearance systems may have implications for several proteinopathies (Aβ, tau, α-synuclein, etc.). Increasing evidence suggests that CSF-mediated waste clearance depends on brain state (wake/sleep), neuronal activity plays an important role,[45,46] and small molecules are cleared via meningeal and extracranial lymphatics; however, several knowledge gaps remain. A central assumption in glymphatic[9,40] and IPAD[41,42] models is that CSF inflow occurs along PVS channels into the parenchyma where mixing with ISF occurs, whereas other mixing models suggest that CSF-ISF exchange occurs directly in the PVS.[43,44] Noninvasive quantitative methods, such as 4D CSF flow, can potentially be used to test these models and shed new light on current controversies.[159]

While glymphatic models suggest outflow along venular and venous PVS, IPAD models suggest outflow along the basement membrane of penetrating arteries and arterioles.[41,42] 4D CSF flow has potential for assessing flow directions in low-flow regions of the SAS and also potentially in dilated PVS, without influencing the flow by pressure gradients induced by contrast injection. Hence, 4D CSF flow may provide insights into

how the SAS is subdivided into influx and efflux routes. However, ISF bulk flow is expected to occur on scales of a few centimeters per day, as shown by studies using intrathecal contrast injection,[160] velocities that are far below what is feasible to capture with PC and 4D flow methods.

Nonquantitative ultrafast fMRI suggests that different frequencies drive CSF flow in different compartments,[52] something that could be further investigated with 4D CSF flow at high field strengths (Figure 12) or with high performance gradient systems (Figure 13). Recent technical developments (on 2.2), such as high field strengths[105] and high performance gradient systems,[106,111] are allowing for high spatiotemporal 4D CSF flow in small SAS compartments with very low velocities (e.g., 1.5-mm isotropic voxel size; $V_{enc} = 1$ cm/s), gated over both cardiac and respiratory cycles. Human PVS detected on MRI typically range from 1 to 4 mm in diameter[161]; however, PVS flow velocities are not entirely known. Animal studies suggest that perivascular CSF bulk motion is driven by cardiac pulsations[50,51] and functional hyperemia,[46] with cardiac-related peak velocities in PVS of mice[51] around 0.02 mm/s. Moreover, a recent human study using a phase-sensitive DTI sequence ($V_{enc} = 0.24$ mm/s) found cardiac-related motion of the order of 0.1 mm/s, potentially representing human PVS flow.[106]

Studies using contrast injections have showed reduced clearance with age.[162,163] Combining such approaches with 4D CSF flow could provide further insights into how the driving mechanisms (e.g., cardiac, respiratory) of CSF motion change during aging and dementia. Finally, 4D flow acquisitions with a wide dynamic range (e.g., dual-V_{enc}; high for CBF and low for CSF velocities) could be used to study the coupling between CBF and CSF dynamics, allowing assessment of altered brain compliance and vascular pumping, which might in turn lead to dysfunctional brain clearance.

3 | SUMMARY AND OUTLOOK

As noted in Figure 2, the annual publication rate of 4D flow MRI continues to increase. This growth is largely driven by both clinical and basic research studies focused on body and cardiothoracic imaging. The publication rate of brain applications is also increasing, albeit at a lower rate, probably because of increased technical demands for high spatiotemporal resolution to assess the smaller vasculature. However, only 24 studies within the last 14 years with "4D flow MRI AND CSF" were found on PubMed, indicating that 4D CSF flow is an understudied research area. The lack of growth in 4D CSF flow studies is partially driven by the challenges discussed in on 2.1, including extended scan times resulting from the long T1 times and low velocities of CSF. While cutting-edge systems with high field strengths and improved gradient performance will certainly drive development and applications of 4D CSF flow in the research realm, technical advances in hardware and software must continue to reduce the data acquisition time and increase velocity sensitivities in the clinical setting. Studies designed to assess reproducibility and repeatability of 4D CSF flow biomarkers and quality control metrics[164] are currently needed to facilitate clinical adoption. True adoption will only be possible after clinical research has established the value of 4D CSF flow-based biomarkers. Is also important to identify 4D CSF flow limitations and the scenarios where 2D PC MRI is preferable (e.g., real-time 2D PC). Technological advances have not only improved 4D flow, but also 2D PC MRI. 4D CSF flow studies could benefit from complementary utilization of 2D PC methods with higher accuracy. Overall, recent technical achievements, as well as the growing interest in understanding brain-clearance pathways and the mechanisms that drive CSF motion, will probably increase the number of 4D CSF flow studies in the future. These ongoing 4D CSF flow developments have the potential to improve our understanding of CSF dynamics in both normal physiology and in various disease states. Such improvements could, in turn, facilitate clinical adoption and the development of new diagnostic and treatment monitoring strategies. Therefore, we recommend being cautiously optimistic about the future of 4D CSF flow.

ACKNOWLEDGMENTS

We acknowledge GE Healthcare for assistance and support. Grant support was provided by the National Institutes of Health (R01AG075788, R01AG027161, R01AG021155, P30AG062715, R21AG077337, R21NS125094, KL2TR002374, and UL1TR002373) and the Alzheimer's Association (AARFD-20-678095).

ORCID

Leonardo A. Rivera-Rivera https://orcid.org/0000-0001-5629-8721

REFERENCES

1. Mestre H, Du T, Sweeney AM, et al. Cerebrospinal fluid influx drives acute ischemic tissue swelling. *Science*. 2020;13;367(6483). doi:10.1126/science.aax7171
2. Tain RW, Bagci AM, Lam BL, Sklar EM, Ertl-Wagner B, Alperin N. Determination of cranio-spinal canal compliance distribution by MRI: methodology and early application in idiopathic intracranial hypertension. *J Magn Reson Imaging*. 2011;34(6):1397-1404. doi:10.1002/jmri.22799
3. Alperin NJ, Lee SH, Loth F, Raksin PB, Lichtor T. MR-intracranial pressure (ICP): a method to measure intracranial elastance and pressure noninvasively by means of MR imaging: baboon and human study. *Radiology*. 2000;217(3):877-885. doi:10.1148/radiology.217.3.r00dc42877
4. Tawfik AM, Elsorogy L, Abdelghaffar R, Naby AA, Elmenshawi I. Phase-contrast MRI CSF flow measurements for the diagnosis of normal-pressure hydrocephalus: observer agreement of velocity versus volume parameters. *Am J Roentgenol*. 2017;208(4):838-843. doi:10.2214/AJR.16.16995

5. Yamada S, Ishikawa M, Ito H, et al. Cerebrospinal fluid dynamics in idiopathic normal pressure hydrocephalus on four-dimensional flow imaging. *Eur Radiol*. 2020;30(8):4454-4465. doi:10.1007/s00330-020-06825-6
6. Bradley WG, Scalzo D, Queralt J, Nitz WN, Atkinson DJ, Wong P. Normal-pressure hydrocephalus: evaluation with cerebrospinal fluid flow measurements at MR imaging. *Radiology*. 1996;198(2):523-529. doi:10.1148/radiology.198.2.8596861
7. El Sankari S, Gondry-Jouet C, Fichten A, et al. Cerebrospinal fluid and blood flow in mild cognitive impairment and Alzheimer's disease: a differential diagnosis from idiopathic normal pressure hydrocephalus. *Fluids Barriers CNS*. 2011;8(1):12. doi:10.1186/2045-8118-8-12
8. de Leon MJ, Li Y, Okamura N, et al. Cerebrospinal fluid clearance in Alzheimer disease measured with dynamic PET. *J Nucl Med*. 2017;58(9):1471-1476. doi:10.2967/jnumed.116.187211
9. Nedergaard M, Goldman SA. Glymphatic failure as a final common pathway to dementia. *Science*. 2020;370(6512):50-56. doi:10.1126/science.abb8739
10. Williams G, Thyagaraj S, Fu A, et al. In vitro evaluation of cerebrospinal fluid velocity measurement in type I Chiari malformation: repeatability, reproducibility, and agreement using 2D phase contrast and 4D flow MRI. *Fluids Barriers CNS*. 2021;18(1):12. doi:10.1186/s12987-021-00246-3
11. Kröger JR, Juettner A, Brentrup A, et al. 4D MR imaging of cerebrospinal fluid flow in Chiari I malformation with and without syringomyelia and flow changes after decompressive surgery. *J Cardiovasc Magn Reson*. 2012;14(Suppl 1):W1. doi:10.1186/1532-429X-14-S1-W1
12. Bunck AC, Kroeger JR, Juettner A, et al. Magnetic resonance 4D flow analysis of cerebrospinal fluid dynamics in Chiari I malformation with and without syringomyelia. *Eur Radiol*. 2012;22(9):1860-1870. doi:10.1007/s00330-012-2457-7
13. Rasmussen MK, Mestre H, Nedergaard M. Fluid transport in the brain. *Physiol Rev*. 2022;102(2):1025-1151. doi:10.1152/physrev.00031.2020
14. Bhadelia RA, Bogdan AR, Kaplan RF, Wolpert SM. Cerebrospinal fluid pulsation amplitude and its quantitative relationship to cerebral blood flow pulsations: a phase-contrast MR flow imaging study. *Neuroradiology*. 1997;39(4):258-264. doi:10.1007/s002340050404
15. Balédent O, Henry-Feugeas MC, Idy-Peretti I. Cerebrospinal fluid dynamics and relation with blood flow: a magnetic resonance study with semiautomated cerebrospinal fluid segmentation. *Invest Radiol*. 2001;36(7):368-377. doi:10.1097/00004424-200107000-00003
16. Tarasoff-Conway JM, Carare RO, Osorio RS, et al. Clearance systems in the brain—implications for Alzheimer disease. *Nat Rev Neurol*. 2015;11(8):457-470. doi:10.1038/nrneurol.2015.119
17. Liu G, Ladrón-de-Guevara A, Izhiman Y, Nedergaard M, Du T. Measurements of cerebrospinal fluid production: a review of the limitations and advantages of current methodologies. *Fluids Barriers CNS*. 2022;19(1):101. doi:10.1186/s12987-022-00382-4
18. Kelley DH, Thomas JH. Cerebrospinal fluid flow. *Annu Rev Fluid Mech*. 2023;55(1):237-264. doi:10.1146/annurev-fluid-120720-011638
19. Eide PK, Valnes LM, Lindstrøm EK, Mardal KA, Ringstad G. Direction and magnitude of cerebrospinal fluid flow vary substantially across central nervous system diseases. *Fluids Barriers CNS*. 2021;18(1):16. doi:10.1186/s12987-021-00251-6
20. Balédent O, Gondry-Jouet C, Meyer ME, et al. Relationship between cerebrospinal fluid and blood dynamics in healthy volunteers and patients with communicating hydrocephalus. *Invest Radiol*. 2004;39(1):45-55. doi:10.1097/01.rli.0000100892.87214.49
21. Proulx ST. Cerebrospinal fluid outflow: a review of the historical and contemporary evidence for arachnoid villi, perineural routes, and dural lymphatics. *Cell Mol Life Sci*. 2021;78(6):2429-2457. doi:10.1007/s00018-020-03706-5
22. Mehta NH, Suss RA, Dyke JP, et al. Quantifying cerebrospinal fluid dynamics: a review of human neuroimaging contributions to CSF physiology and neurodegenerative disease. *Neurobiol Dis*. 2022;170:105776. doi:10.1016/j.nbd.2022.105776
23. Santini F, Wetzel SG, Bock J, Markl M, Scheffler K. Time-resolved three-dimensional (3D) phase-contrast (PC) balanced steady-state free precession (bSSFP). *Magn Reson Med*. 2009;62(4):966-974. doi:10.1002/mrm.22087
24. Bunck AC, Kröger JR, Jüttner A, et al. Magnetic resonance 4D flow characteristics of cerebrospinal fluid at the craniocervical junction and the cervical spinal canal. *Eur Radiol*. 2011;21(8):1788-1796. doi:10.1007/s00330-011-2105-7
25. Odéen H, Uppman M, Markl M, Spottiswoode BS. Assessing cerebrospinal fluid flow connectivity using 3D gradient echo phase contrast velocity encoded MRI. *Physiol Meas*. 2011;32(4):407-421. doi:10.1088/0967-3334/32/4/003
26. Stadlbauer A, Salomonowitz E, Brenneis C, et al. Magnetic resonance velocity mapping of 3D cerebrospinal fluid flow dynamics in hydrocephalus: preliminary results. *Eur Radiol*. 2012;22(1):232-242. doi:10.1007/s00330-011-2247-7
27. Yiallourou TI, Kröger JR, Stergiopulos N, Maintz D, Martin BA, Bunck AC. Comparison of 4D phase-contrast MRI flow measurements to computational fluid dynamics simulations of cerebrospinal fluid motion in the cervical spine. *PLoS ONE*. 2012;7(12):e52284. doi:10.1371/journal.pone.0052284
28. Matsumae M, Hirayama A, Atsumi H, Yatsushiro S, Kuroda K. Velocity and pressure gradients of cerebrospinal fluid assessed with magnetic resonance imaging. *J Neurosurg*. 2014;120(1):218-227. doi:10.3171/2013.7.JNS121859
29. Hirayama A, Matsumae M, Yatsushiro S, Abdulla A, Atsumi H, Kuroda K. Visualization of pulsatile CSF motion around membrane-like structures with both 4D velocity mapping and time-SLIP technique. *Magn Reson Med Sci*. 2015;14(4):263-273. doi:10.2463/mrms.2014-0089
30. Heidari Pahlavian S, Bunck AC, Loth F, et al. Characterization of the discrepancies between four-dimensional phase-contrast magnetic resonance imaging and in-silico simulations of cerebrospinal fluid dynamics. *J Biomech Eng*. 2015;137(5):051002. doi:10.1115/1.4029699
31. Heidari Pahlavian S, Bunck AC, Thyagaraj S, et al. Accuracy of 4D flow measurement of cerebrospinal fluid dynamics in the cervical spine: an in vitro verification against numerical simulation. *Ann Biomed Eng*. 2016;44(11):3202-3214. doi:10.1007/s10439-016-1602-x
32. Thyagaraj S, Pahlavian SH, Sass LR, et al. An MRI-compatible hydrodynamic simulator of cerebrospinal fluid motion in the cervical spine. *IEEE Trans Biomed Eng*. 2018;65(7):1516-1523. doi:10.1109/TBME.2017.2756995
33. Takizawa K, Matsumae M, Hayashi N, Hirayama A, Yatsushiro S, Kuroda K. Hyperdynamic CSF motion profiles found in idiopathic normal pressure hydrocephalus and Alzheimer's disease assessed by fluid mechanics derived from magnetic resonance images. *Fluids Barriers CNS*. 2017;14(1):29. doi:10.1186/s12987-017-0077-y
34. Takizawa K, Matsumae M, Hayashi N, et al. The choroid plexus of the lateral ventricle as the origin of CSF pulsation is questionable. *Neurol Med Chir*. 2018;58(1):23-31. doi:10.2176/nmc.oa.2017-0117
35. Brandner S, Buchfelder M, Eyuepoglu IY, Luecking H, Doerfler A, Stadlbauer A. Visualization of CSF flow with time-resolved 3D MR velocity mapping in aqueductal stenosis before and after endoscopic third ventriculostomy: a feasibility study. *Clin Neuroradiol*. 2018;28(1):69-74. doi:10.1007/s00062-016-0530-3
36. Yatsushiro S, Sunohara S, Hayashi N, et al. Cardiac-driven pulsatile motion of intracranial cerebrospinal fluid visualized based on a correlation mapping technique. *Magn Reson Med Sci*. 2018;17(2):151-160. doi:10.2463/mrms.mp.2017-0014

37. Jaeger E, Sonnabend K, Schaarschmidt F, Maintz D, Weiss K, Bunck AC. Compressed-sensing accelerated 4D flow MRI of cerebrospinal fluid dynamics. *Fluids Barriers CNS*. 2020;17(1):43. doi:10.1186/s12987-020-00206-3
38. Yamada S, Ito H, Ishikawa M, et al. Quantification of oscillatory shear stress from reciprocating CSF motion on 4D flow imaging. *Am J Neuroradiol*. 2021;42(3):479-486. doi:10.3174/ajnr.A6941
39. Yavuz Ilik S, Otani T, Yamada S, Watanabe Y, Wada S. A subject-specific assessment of measurement errors and their correction in cerebrospinal fluid velocity maps using 4D flow MRI. *Magn Reson Med*. 2022;87(5):2412-2423. doi:10.1002/mrm.29111
40. Iliff JJ, Wang M, Liao Y, et al. A paravascular pathway facilitates CSF flow through the brain parenchyma and the clearance of interstitial solutes, including amyloid β. *Sci Transl Med*. 2012;4(147):147ra111. doi:10.1126/scitranslmed.3003748
41. Hawkes CA, Jayakody N, Johnston DA, Bechmann I, Carare RO. Failure of perivascular drainage of β-amyloid in cerebral amyloid angiopathy. *Brain Pathol*. 2014;24(4):396-403. doi:10.1111/bpa.12159
42. Aldea R, Weller RO, Wilcock DM, Carare RO, Richardson G. Cerebrovascular smooth muscle cells as the drivers of intramural periarterial drainage of the brain. *Front Aging Neurosci*. 2019;11:1. doi:10.3389/fnagi.2019.00001
43. Bakker ENTP, Naessens DMP, VanBavel E. Paravascular spaces: entry to or exit from the brain? *Exp Physiol*. 2019;104(7):1013-1017. doi:10.1113/EP087424
44. Zhao L, Tannenbaum A, Bakker ENTP, Benveniste H. Physiology of glymphatic solute transport and waste clearance from the brain. *Phys Ther*. 2022;37(6):349-362. doi:10.1152/physiol.00015.2022
45. Fultz NE, Bonmassar G, Setsompop K, et al. Coupled electrophysiological, hemodynamic, and cerebrospinal fluid oscillations in human sleep. *Science*. 2019;366(6465):628-631. doi:10.1126/science.aax5440
46. van Veluw SJ, Hou SS, Calvo-Rodriguez M, et al. Vasomotion as a driving force for paravascular clearance in the awake mouse brain. *Neuron*. 2020;105(3):549-561.e5. doi:10.1016/j.neuron.2019.10.033
47. Dreha-Kulaczewski S, Konopka M, Joseph AA, et al. Respiration and the watershed of spinal CSF flow in humans. *Sci Rep*. 2018;8(1):5594. doi:10.1038/s41598-018-23908-z
48. Baselli G, Fasani F, Pelizzari L, Cazzoli M, Baglio F, Laganà MM. Real-time phase-contrast MRI to monitor cervical blood and cerebrospinal fluid flow beat-by-beat variability. *Biosensors*. 2022;12(6):417. doi:10.3390/bios12060417
49. Laganà MM, Di Tella S, Ferrari F, et al. Blood and cerebrospinal fluid flow oscillations measured with real-time phase-contrast MRI: breathing mode matters. *Fluids Barriers CNS*. 2022;19(1):100. doi:10.1186/s12987-022-00394-0
50. Iliff JJ, Wang M, Zeppenfeld DM, et al. Cerebral arterial pulsation drives paravascular CSF-interstitial fluid exchange in the murine brain. *J Neurosci*. 2013;33(46):18190-18199. doi:10.1523/JNEUROSCI.1592-13.2013
51. Mestre H, Tithof J, Du T, et al. Flow of cerebrospinal fluid is driven by arterial pulsations and is reduced in hypertension. *Nat Commun*. 2018;9(1):4878. doi:10.1038/s41467-018-07318-3
52. Kiviniemi V, Wang X, Korhonen V, et al. Ultra-fast magnetic resonance encephalography of physiological brain activity-glymphatic pulsation mechanisms? *J Cereb Blood Flow Metab*. 2016;36(6):1033-1045. doi:10.1177/0271678X15622047
53. Dumoulin CL, Souza SP, Walker MF, Wagle W. Three-dimensional phase contrast angiography. *Magn Reson Med*. 1989;9(1):139-149. doi:10.1002/mrm.1910090117
54. Markl M, Frydrychowicz A, Kozerke S, Hope M, Wieben O. 4D flow MRI. *J Magn Reson Imaging*. 2012;36(5):1015-1036. doi:10.1002/jmri.23632
55. Pelc NJ, Herfkens RJ, Shimakawa A, Enzmann DR. Phase contrast cine magnetic resonance imaging. *Magn Reson Q*. 1991;7(4):229-254.
56. Moran PR. A flow velocity zeugmatographic interlace for NMR imaging in humans. *Magn Reson Imaging*. 1982;1(4):197-203. doi:10.1016/0730-725X(82)90170-9
57. Feinberg DA, Mark AS. Human brain motion and cerebrospinal fluid circulation demonstrated with MR velocity imaging. *Radiology*. 1987;163(3):793-799. doi:10.1148/radiology.163.3.3575734
58. Wåhlin A, Ambarki K, Birgander R, Malm J, Eklund A. Intracranial pulsatility is associated with regional brain volume in elderly individuals. *Neurobiol Aging*. 2014;35(2):365-372. doi:10.1016/j.neurobiolaging.2013.08.026
59. Kaipainen AL, Martoma E, Puustinen T, et al. Cerebrospinal fluid dynamics in idiopathic intracranial hypertension: a literature review and validation of contemporary findings. *Acta Neurochir*. 2021;163(12):3353-3368. doi:10.1007/s00701-021-04940-x
60. Wolf K, Luetzen N, Mast H, et al. CSF flow and spinal cord motion in patients with spontaneous intracranial hypotension: a phase contrast MRI study. *Neurology*. 2023;100(7):e651-e660. doi:10.1212/WNL.0000000000201527
61. Pinna G, Alessandrini F, Alfieri A, Rossi M, Bricolo A. Cerebrospinal fluid flow dynamics study in Chiari I malformation: implications for syrinx formation. *Neurosurg Focus*. 2000;8(3):1-8. doi:10.3171/foc.2000.8.3.3
62. Mohammad SA, Osman NM, Ahmed KA. The value of CSF flow studies in the management of CSF disorders in children: a pictorial review. *Insights Imaging*. 2019;10(1):3. doi:10.1186/s13244-019-0686-x
63. Soulat G, McCarthy P, Markl M. 4D flow with MRI. *Annu Rev Biomed Eng*. 2020;22:103-126. doi:10.1146/annurev-bioeng-100219-110055
64. Oechtering TH, Roberts GS, Panagiotopoulos N, Wieben O, Roldán-Alzate A, Reeder SB. Abdominal applications of quantitative 4D flow MRI. *Abdom Radiol*. 2022;47(9):3229-3250. doi:10.1007/s00261-021-03352-w
65. Ngo MT, Kim CI, Jung J, Chung GH, Lee DH, Kwak HS. Four-dimensional flow magnetic resonance imaging for assessment of velocity magnitudes and flow patterns in the human carotid artery bifurcation: comparison with computational fluid dynamics. *Diagnostics*. 2019;9(4):223. doi:10.3390/diagnostics9040223
66. Schnell S, Wu C, Ansari SA. Four-dimensional MRI flow examinations in cerebral and extracerebral vessels—ready for clinical routine? *Curr Opin Neurol*. 2016;29(4):419-428. doi:10.1097/WCO.0000000000000341
67. Turski P, Scarano A, Hartman E, et al. Neurovascular 4DFlow MRI (phase contrast MRA): emerging clinical applications. *Neurovasc Imag*. 2016;2(1):8. doi:10.1186/s40809-016-0019-0
68. Wåhlin A, Eklund A, Malm J. 4D flow MRI hemodynamic biomarkers for cerebrovascular diseases. *J Intern Med*. 2022;291(2):115-127. doi:10.1111/joim.13392
69. Morgan AG, Thrippleton MJ, Wardlaw JM, Marshall I. 4D flow MRI for non-invasive measurement of blood flow in the brain: a systematic review. *J Cereb Blood Flow Metab*. 2021;41(2):206-218. doi:10.1177/0271678X20952014

70. Bissell MM, Raimondi F, Ait Ali L, et al. 4D Flow cardiovascular magnetic resonance consensus statement: 2023 update. *J Cardiovasc Magn Reson*. 2023;25(1):40. doi:10.1186/s12968-023-00942-z
71. Ehman RL, Felmlee JP. Adaptive technique for high-definition MR imaging of moving structures. *Radiology*. 1989;173(1):255-263. doi:10.1148/radiology.173.1.2781017
72. McConnell MV, Khasgiwala VC, Savord BJ, et al. Comparison of respiratory suppression methods and navigator locations for MR coronary angiography. *Am J Roentgenol*. 1997;168(5):1369-1375. doi:10.2214/ajr.168.5.9129447
73. Uribe S, Beerbaum P, Sørensen TS, Rasmusson A, Razavi R, Schaeffter T. Four-dimensional (4D) flow of the whole heart and great vessels using real-time respiratory self-gating. *Magn Reson Med*. 2009;62(4):984-992. doi:10.1002/mrm.22090
74. Maier SE, Hardy CJ, Jolesz FA. Brain and cerebrospinal fluid motion: real-time quantification with M-mode MR imaging. *Radiology*. 1994;193(2):477-483. doi:10.1148/radiology.193.2.7972766
75. Töger J, Andersen M, Haglund O, Kylkilahti TM, Lundgaard I, Markenroth BK. Real-time imaging of respiratory effects on cerebrospinal fluid flow in small diameter passageways. *Magn Reson Med*. 2022;88(2):770-786. doi:10.1002/mrm.29248
76. Johnson KM, Lum DP, Turski PA, Block WF, Mistretta CA, Wieben O. Improved 3D phase contrast MRI with off-resonance corrected dual echo VIPR. *Magn Reson Med*. 2008;60(6):1329-1336. doi:10.1002/mrm.21763
77. Schnell S, Ansari SA, Wu C, et al. Accelerated dual-venc 4D flow MRI for neurovascular applications. *J Magn Reson Imaging*. 2017;46(1):102-114. doi:10.1002/jmri.25595
78. Aristova M, Pang J, Ma Y, et al. Accelerated dual-venc 4D flow MRI with variable high-venc spatial resolution for neurovascular applications. *Magn Reson Med*. 2022;88(4):1643-1658. doi:10.1002/mrm.29306
79. Johnson KM, Markl M. Improved SNR in phase contrast velocimetry with five-point balanced flow encoding. *Magn Reson Med*. 2010;63(2):349-355. doi:10.1002/mrm.22202
80. Rivera-Rivera LA, Cody KA, Eisenmenger L, et al. Assessment of vascular stiffness in the internal carotid artery proximal to the carotid canal in Alzheimer's disease using pulse wave velocity from low rank reconstructed 4D flow MRI. *J Cereb Blood Flow Metab*. 2021;41(2):298-311. doi:10.1177/0271678X20910302
81. Kim D, Jen ML, Eisenmenger LB, Johnson KM. Accelerated 4D-flow MRI with 3-point encoding enabled by machine learning. *Magn Reson Med*. 2023;89(2):800-811. doi:10.1002/mrm.29469
82. Schrauben E, Wåhlin A, Ambarki K, et al. Fast 4D flow MRI intracranial segmentation and quantification in tortuous arteries. *J Magn Reson Imaging*. 2015;42(5):1458-1464. doi:10.1002/jmri.24900
83. Vali A, Aristova M, Vakil P, et al. Semi-automated analysis of 4D flow MRI to assess the hemodynamic impact of intracranial atherosclerotic disease. *Magn Reson Med*. 2019;82(2):749-762. doi:10.1002/mrm.27747
84. Vikner T, Nyberg L, Holmgren M, Malm J, Eklund A, Wåhlin A. Characterizing pulsatility in distal cerebral arteries using 4D flow MRI. *J Cereb Blood Flow Metab*. 2020;40(12):2429-2440. doi:10.1177/0271678X19886667
85. Roberts GS, Hoffman CA, Rivera-Rivera LA, Berman SE, Eisenmenger LB, Wieben O. Automated hemodynamic assessment for cranial 4D flow MRI. *Magn Reson Imaging*. 2023;97:46-55. doi:10.1016/j.mri.2022.12.016
86. Vikner T, Karalija N, Eklund A, et al. 5-year associations among cerebral arterial pulsatility, perivascular space dilation, and white matter lesions. *Ann Neurol*. 2022;92(5):871-881. doi:10.1002/ana.26475
87. Björnfot C, Garpebring A, Qvarlander S, Malm J, Eklund A, Wåhlin A. Assessing cerebral arterial pulse wave velocity using 4D flow MRI. *J Cereb Blood Flow Metab*. 2021;41(10):2769-2777. doi:10.1177/0271678X211008744
88. Vikner T, Eklund A, Karalija N, et al. Cerebral arterial pulsatility is linked to hippocampal microvascular function and episodic memory in healthy older adults. *J Cereb Blood Flow Metab*. 2021;41(7):1778-1790. doi:10.1177/0271678X20980652
89. Rivera-Rivera LA, Turski P, Johnson KM, et al. 4D flow MRI for intracranial hemodynamics assessment in Alzheimer's disease. *J Cereb Blood Flow Metab*. 2016;36(10):1718-1730. doi:10.1177/0271678X15617171
90. Berman SE, Rivera-Rivera LA, Clark LR, et al. Intracranial arterial four-dimensional flow is associated with metrics of brain health and Alzheimer's disease. *Alzheimers Dement*. 2015;1(4):420-428. doi:10.1016/j.dadm.2015.09.005
91. Clark LR, Berman SE, Rivera-Rivera LA, et al. Macrovascular and microvascular cerebral blood flow in adults at risk for Alzheimer's disease. *Alzheimers Dement*. 2017;7:48-55. doi:10.1016/j.dadm.2017.01.002
92. Rivera-Rivera LA, Eisenmenger L, Cody KA, et al. Cerebrovascular stiffness and flow dynamics in the presence of amyloid and tau biomarkers. *Alzheimers Dement*. 2021;13(1):e12253. doi:10.1002/dad2.12253
93. Zhang X, Petersen ET, Ghariq E, et al. In vivo blood T_1 measurements at 1.5 T, 3 T, and 7 T. *Magn Reson Med*. 2013;70(4):1082-1086. doi:10.1002/mrm.24550
94. Bojorquez JZ, Bricq S, Acquitter C, Brunotte F, Walker PM, Lalande A. What are normal relaxation times of tissues at 3 T? *Magn Reson Imaging*. 2017;35:69-80. doi:10.1016/j.mri.2016.08.021
95. Rooney WD, Johnson G, Li X, et al. Magnetic field and tissue dependencies of human brain longitudinal ^1H_2O relaxation in vivo. *Magn Reson Med*. 2007;57(2):308-318. doi:10.1002/mrm.21122
96. Markl M, Leupold J. Gradient echo imaging. *J Magn Reson Imaging*. 2012;35(6):1274-1289. doi:10.1002/jmri.23638
97. Hargreaves BA. Rapid gradient-echo imaging. *J Magn Reson Imaging*. 2012;36(6):1300-1313. doi:10.1002/jmri.23742
98. Lee AT, Bruce Pike G, Pelc NJ. Three-point phase-contrast velocity measurements with increased velocity-to-noise ratio. *Magn Reson Med*. 1995;33(1):122-126. doi:10.1002/mrm.1910330119
99. McCormack EJ, Egnor MR, Wagshul ME. Improved cerebrospinal fluid flow measurements using phase contrast balanced steady-state free precession. *Magn Reson Imaging*. 2007;25(2):172-182. doi:10.1016/j.mri.2006.09.023
100. Markl M, Alley MT, Pelc NJ. Balanced phase-contrast steady-state free precession (PC-SSFP): a novel technique for velocity encoding by gradient inversion. *Magn Reson Med*. 2003;49(5):945-952. doi:10.1002/mrm.10451
101. Bieri O, Scheffler K. Fundamentals of balanced steady state free precession MRI. *J Magn Reson Imaging*. 2013;38(1):2-11. doi:10.1002/jmri.24163
102. Spijkerman JM, Petersen ET, Hendrikse J, Luijten P, Zwanenburg JJM. T_2 mapping of cerebrospinal fluid: 3 T versus 7 T. *MAGMA*. 2018;31(3):415-424. doi:10.1007/s10334-017-0659-3

103. Kim D, Eisenmenger L, Turski P, Johnson KM. Simultaneous 3D-TOF angiography and 4D-flow MRI with enhanced flow signal using multiple overlapping thin slab acquisition and magnetization transfer. *Magn Reson Med*. 2022;87(3):1401-1417. doi:10.1002/mrm.29060
104. Sakhare AR, Barisano G, Pa J. Assessing test–retest reliability of phase contrast MRI for measuring cerebrospinal fluid and cerebral blood flow dynamics. *Magn Reson Med*. 2019;82(2):658-670. doi:10.1002/mrm.27752
105. Dong Z, Wang F, Strom AK, et al. 4D whole-brain CSF flowmetry: slow flow dynamics in ventricles and subarachnoid space. ISMRM Workshop on Neurofluids: Anatomy, Physiology & Imaging, 21–24 September 2022, Sapienza University of Rome, Rome, Italy. 2022.
106. Shih RY, DeMarco JK, Werner JK, et al. Cyclic intracerebral coherent motion on peripheral-pulse-gated ultra-low VENC MRI: noninvasive depiction of glymphatic flow? *Proc Intl Soc Mag Reson Med*. 2020;28:0645.
107. Battal B, Kocaoglu M, Bulakbasi N, Husmen G, Tuba Sanal H, Tayfun C. Cerebrospinal fluid flow imaging by using phase-contrast MR technique. *Br J Radiol*. 2011;84(1004):758-765. doi:10.1259/bjr/66206791
108. Gupta S, Soellinger M, Grzybowski DM, et al. Cerebrospinal fluid dynamics in the human cranial subarachnoid space: an overlooked mediator of cerebral disease. I. Computational model. *J R Soc Interface*. 2010;7(49):1195-1204. doi:10.1098/rsif.2010.0033
109. Youn SW, Lee J. From 2D to 4D phase-contrast MRI in the neurovascular system: will it be a quantum jump or a fancy decoration? *J Magn Reson Imaging*. 2022;55(2):347-372. doi:10.1002/jmri.27430
110. Roberts GS, Peret A, Jonaitis EM, et al. Normative cerebral hemodynamics in middle-aged and older adults using 4D flow MRI: initial analysis of vascular aging. *Radiology*. 2023;307(3):e222685. doi:10.1148/radiol.222685
111. Foo TKF, Tan ET, Vermilyea ME, et al. Highly efficient head-only magnetic field insert gradient coil for achieving simultaneous high gradient amplitude and slew rate at 3.0T (MAGNUS) for brain microstructure imaging. *Magn Reson Med*. 2020;83(6):2356-2369. doi:10.1002/mrm.28087
112. Loecher M, Schrauben E, Johnson KM, Wieben O. Phase unwrapping in 4D MR flow with a 4D single-step laplacian algorithm. *J Magn Reson Imaging*. 2016;43(4):833-842. doi:10.1002/jmri.25045
113. Lorenz R, Bock J, Snyder J, Korvink JG, Jung BA, Markl M. Influence of eddy current, Maxwell and gradient field corrections on 3D flow visualization of 3D CINE PC-MRI data. *Magn Reson Med*. 2014;72(1):33-40. doi:10.1002/mrm.24885
114. Wentland AL, Wieben O, Korosec FR, Haughton VM. Accuracy and reproducibility of phase-contrast MR imaging measurements for CSF flow. *Am J Neuroradiol*. 2010;31(7):1331-1336. doi:10.3174/ajnr.A2039
115. Busch J, Giese D, Kozerke S. Image-based background phase error correction in 4D flow MRI revisited. *J Magn Reson Imaging*. 2017;46(5):1516-1525. doi:10.1002/jmri.25668
116. Dillinger H, Walheim J, Kozerke S. On the limitations of echo planar 4D flow MRI. *Magn Reson Med*. 2020;84(4):1806-1816. doi:10.1002/mrm.28236
117. Peters DC, Korosec FR, Grist TM, et al. Undersampled projection reconstruction applied to MR angiography. *Magn Reson Med*. 2000;43(1):91-101. doi:10.1002/(sici)1522-2594(200001)43:13.0.co;2-4
118. Barger AV, Block WF, Toropov Y, Grist TM, Mistretta CA. Time-resolved contrast-enhanced imaging with isotropic resolution and broad coverage using an undersampled 3D projection trajectory. *Magn Reson Med*. 2002;48(2):297-305. doi:10.1002/mrm.10212
119. Sigfridsson A, Petersson S, Carlhäll CJ, Ebbers T. Four-dimensional flow MRI using spiral acquisition. *Magn Reson Med*. 2012;68(4):1065-1073. doi:10.1002/mrm.23297
120. Steinman DA, Ethier CR, Rutt BK. Combined analysis of spatial and velocity displacement artifacts in phase contrast measurements of complex flows. *J Magn Reson Imaging*. 1997;7(2):339-346. doi:10.1002/jmri.1880070214
121. Lee Y, Wilm BJ, Brunner DO, et al. On the signal-to-noise ratio benefit of spiral acquisition in diffusion MRI. *Magn Reson Med*. 2021;85(4):1924-1937. doi:10.1002/mrm.28554
122. Glover GH. Spiral imaging in fMRI. *Neuroimage*. 2012;62(2):706-712. doi:10.1016/j.neuroimage.2011.10.039
123. Petersson S, Sigfridsson A, Dyverfeldt P, Carlhäll CJ, Ebbers T. Retrospectively gated intracardiac 4D flow MRI using spiral trajectories. *Magn Reson Med*. 2016;75(1):196-206. doi:10.1002/mrm.25612
124. Engel M, Kasper L, Barmet C, et al. Single-shot spiral imaging at 7 T. *Magn Reson Med*. 2018;80(5):1836-1846. doi:10.1002/mrm.27176
125. Glover GH, Pauly JM. Projection reconstruction techniques for reduction of motion effects in MRI. *Magn Reson Med*. 1992;28(2):275-289. doi:10.1002/mrm.1910280209
126. Johnson KM, Fain SB, Schiebler ML, Nagle S. Optimized 3D ultrashort echo time pulmonary MRI. *Magn Reson Med*. 2013;70(5):1241-1250. doi:10.1002/mrm.24570
127. Kecskemeti S, Samsonov A, Hurley SA, Dean DC, Field A, Alexander AL. MPnRAGE: a technique to simultaneously acquire hundreds of differently contrasted MPRAGE images with applications to quantitative T1 mapping. *Magn Reson Med*. 2016;75(3):1040-1053. doi:10.1002/mrm.25674
128. Anderson AG, Velikina J, Block W, Wieben O, Samsonov A. Adaptive retrospective correction of motion artifacts in cranial MRI with multicoil three-dimensional radial acquisitions. *Magn Reson Med*. 2013;69(4):1094-1103. doi:10.1002/mrm.24348
129. Rivera-Rivera LA, Kecskemeti S, Jen ML, et al. Motion-corrected 4D-Flow MRI for neurovascular applications. *Neuroimage*. 2022;264:119711. doi:10.1016/j.neuroimage.2022.119711
130. Anderson AG III, Velikina J, Wieben O, Samsonov A. Motion correction for 3D phase contrast flow imaging with cranial PCVIPR. In: *Proceedings of the International Society for Magnetic Resonance in Medicine*. Vol.20; 2012:3415.The ISMRM.
131. Spijkerman JM, Geurts LJ, Siero JCW, Hendrikse J, Luijten PR, Zwanenburg JJM. Phase contrast MRI measurements of net cerebrospinal fluid flow through the cerebral aqueduct are confounded by respiration. *J Magn Reson Imaging*. 2019;49(2):433-444. doi:10.1002/jmri.26181
132. Yatsushiro S, Sunohara S, Tokushima T, et al. Characterization of cardiac- and respiratory-driven cerebrospinal fluid motions using a correlation mapping technique based on asynchronous two-dimensional phase contrast MR imaging. *Magn Reson Med Sci*. 2021;20(4):385-395. doi:10.2463/mrms.mp.2020-0085
133. Dreha-Kulaczewski S, Joseph AA, Merboldt KD, Ludwig HC, Gärtner J, Frahm J. Inspiration is the major regulator of human CSF flow. *J Neurosci*. 2015;35(6):2485-2491. doi:10.1523/JNEUROSCI.3246-14.2015
134. Nayak KS, Lim Y, Campbell-Washburn AE, Steeden J. Real-time magnetic resonance imaging. *J Magn Reson Imaging*. 2022;55(1):81-99. doi:10.1002/jmri.27411
135. Bert RJ, Settipalle N, Muddasani D, et al. ECG gating is more precise than peripheral pulse gating when quantifying spinal CSF pulsations using phase contrast cine MRI. *Acad Radiol*. 2020;27(4):552-562. doi:10.1016/j.acra.2019.06.015

136. Ludwig J, Speier P, Seifert F, Schaeffter T, Kolbitsch C. Pilot tone-based motion correction for prospective respiratory compensated cardiac cine MRI. *Magn Reson Med*. 2021;85(5):2403-2416. doi:10.1002/mrm.28580
137. Anand S, Lustig M. Beat pilot tone: versatile, contact-free motion sensing in MRI with radio frequency intermodulation. arXiv Preprint posted online June 17, 2023. doi:10.48550/arXiv.2306.10236
138. Lin K, Sarnari R, Speier P, et al. Pilot tone-triggered MRI for quantitative assessment of cardiac function, motion, and structure. *Invest Radiol*. 2023;58(3):239-243. doi:10.1097/RLI.0000000000000922
139. Hurd ER, Han M, Mendes JK, et al. Comparison of prospective and retrospective gated 4D flow cardiac MR image acquisitions in the carotid bifurcation. *Cardiovasc Eng Technol*. 2023;14(1):1-12. doi:10.1007/s13239-022-00630-6
140. Velikina JV, Johnson KM, Wu Y, Samsonov AA, Turski P, Mistretta CA. PC HYPR flow: a technique for rapid imaging of contrast dynamics. *J Magn Reson Imaging*. 2010;31(2):447-456. doi:10.1002/jmri.22035
141. Polzin JA, Frayne R, Grist TM, Mistretta CA. Frequency response of multi-phase segmented k-space phase-contrast. *Magn Reson Med*. 1996;35(5):755-762. doi:10.1002/mrm.1910350517
142. Long D, McMurdo C, Ferdian E, et al. Super-resolution 4D flow MRI to quantify aortic regurgitation using computational fluid dynamics and deep learning. *Int J Cardiovasc Imaging*. 2023;39(6):1189-1202. doi:10.1007/s10554-023-02815-z
143. Ferdian E, Suinesiaputra A, Dubowitz DJ, et al. 4DFlowNet: super-resolution 4D flow MRI using deep learning and computational fluid dynamics. *Front Physiol*. 2020;8:138. doi:10.3389/fphy.2020.00138
144. Peper ES, Van Ooij P, Jung B, Huber A, Gräni C, Bastiaansen JAM. Advances in machine learning applications for cardiovascular 4D flow MRI. *Front Cardiovasc Med*. 2022;9:1052068. doi:10.3389/fcvm.2022.1052068
145. Rutkowski DR, Roldán-Alzate A, Johnson KM. Enhancement of cerebrovascular 4D flow MRI velocity fields using machine learning and computational fluid dynamics simulation data. *Sci Rep*. 2021;11(1):10240. doi:10.1038/s41598-021-89636-z
146. Shit S, Zimmermann J, Ezhov I, et al. SRflow: deep learning based super-resolution of 4D-flow MRI data. *Front Artif Intell*. 2022;5:928181. doi:10.3389/frai.2022.928181
147. Williamson NH, Komlosh ME, Benjamini D, Basser PJ. Limits to flow detection in phase contrast MRI. *J Magn Reson Open*. 2020;2-3:100004. doi:10.1016/j.jmro.2020.100004
148. Magdoom KN, Zeinomar A, Lonser RR, Sarntinoranont M, Mareci TH. Phase contrast MRI of creeping flows using stimulated echo. *J Magn Reson*. 2019;299:49-58. doi:10.1016/j.jmr.2018.12.009
149. Oechtering TH, Nowak A, Sieren MM, et al. Repeatability and reproducibility of various 4D Flow MRI postprocessing software programs in a multi-software and multi-vendor cross-over comparison study. *J Cardiovasc Magn Reson*. 2023;25(1):22. doi:10.1186/s12968-023-00921-4
150. Williams MA, Malm J. Diagnosis and treatment of idiopathic normal pressure hydrocephalus. *Continuum*. 2016;22(2, Dementia):579-599. doi:10.1212/CON.0000000000000305
151. Bradley WGJ. CSF flow in the brain in the context of normal pressure hydrocephalus. *Am J Neuroradiol*. 2015;36(5):831-838. doi:10.3174/ajnr.A4124
152. Yamada S, Tsuchiya K, Bradley WG, et al. Current and emerging MR imaging techniques for the diagnosis and management of CSF flow disorders: a review of phase-contrast and time-spatial labeling inversion pulse. *Am J Neuroradiol*. 2015;36(4):623-630. doi:10.3174/ajnr.A4030
153. Ringstad G, Vatnehol SAS, Eide PK. Glymphatic MRI in idiopathic normal pressure hydrocephalus. *Brain*. 2017;140(10):2691-2705. doi:10.1093/brain/awx191
154. Mihalj M, Dolić K, Kolić K, Ledenko V. CSF tap test—obsolete or appropriate test for predicting shunt responsiveness? A systemic review. *J Neurol Sci*. 2016;362:78-84. doi:10.1016/j.jns.2016.01.028
155. Lindstrøm EK, Ringstad G, Mardal KA, Eide PK. Cerebrospinal fluid volumetric net flow rate and direction in idiopathic normal pressure hydrocephalus. *Neuroimage Clin*. 2018;20:731-741. doi:10.1016/j.nicl.2018.09.006
156. Egnor M, Zheng L, Rosiello A, Gutman F, Davis R. A model of pulsations in communicating hydrocephalus. *Pediatr Neurosurg*. 2002;36(6):281-303. doi:10.1159/000063533
157. Greitz D. Radiological assessment of hydrocephalus: new theories and implications for therapy. *Neurosurg Rev*. 2004;27(3):145-165; discussion 166-167. doi:10.1007/s10143-004-0326-9
158. Bhadelia RA, Chang YM, Oshinski JN, Loth F. Cerebrospinal fluid flow and brain motion in Chiari I malformation: past, present, and future. *J Magn Reson Imaging*. 2023;58(2):360-378. doi:10.1002/jmri.28717
159. Bohr T, Hjorth PG, Holst SC, et al. The glymphatic system: current understanding and modeling. *iScience*. 2022;25(9):104987. doi:10.1016/j.isci.2022.104987
160. Ringstad G, Valnes LM, Dale AM, et al. Brain-wide glymphatic enhancement and clearance in humans assessed with MRI. *JCI Insight*. 2018;3(13):e121537. doi:10.1172/jci.insight.121537
161. Lynch KM, Sepehrband F, Toga AW, Choupan J. Brain perivascular space imaging across the human lifespan. *Neuroimage*. 2023;271:120009. doi:10.1016/j.neuroimage.2023.120009
162. Kress BT, Iliff JJ, Xia M, et al. Impairment of paravascular clearance pathways in the aging brain. *Ann Neurol*. 2014;76(6):845-861. doi:10.1002/ana.24271
163. Zhou Y, Cai J, Zhang W, et al. Impairment of the glymphatic pathway and putative meningeal lymphatic vessels in the aging human. *Ann Neurol*. 2020;87(3):357-369. doi:10.1002/ana.25670
164. Isoda H, Fukuyama A. Quality control for 4D flow MR imaging. *Magn Reson Med Sci*. 2022;21(2):278-292. doi:10.2463/mrms.rev.2021-0165

How to cite this article: Rivera-Rivera LA, Vikner T, Eisenmenger L, Johnson SC, Johnson KM. Four-dimensional flow MRI for quantitative assessment of cerebrospinal fluid dynamics: Status and opportunities. *NMR in Biomedicine*. 2024;37(7):e5082. doi:10.1002/nbm.5082